Mediator Kinase Phosphorylation of STAT1 S727 Promotes Growth of Neoplasms With JAK-STAT Activation

EBioMedicine 26 (2017) 112–125

Contents lists available at ScienceDirect

EBioMedicine

journal homepage: www.ebiomedicine.com

Research Paper

Mediator Kinase Phosphorylation of STAT1 S727 Promotes Growth of Neoplasms With JAK-STAT Activation

Ioana I. Nitulescu [a], Sara C. Meyer [b], Qiang Jeremy Wen [c], John D. Crispino [c], Madeleine E. Lemieux [d], Ross L. Levine [e], Henry E. Pelish [a], Matthew D. Shair [a,*]

[a] Department of Chemistry and Chemical Biology, Harvard University, Cambridge, MA 02138, USA
[b] Human Oncology and Pathogenesis Program, Memorial Sloan Kettering Cancer Center, New York, NY 10065, USA
[c] Division of Hematology and Oncology, Department of Medicine, Northwestern University, Chicago, IL, USA
[d] Bioinfo, Plantagenet, Ontario K0B 1L0, Canada
[e] Leukemia Service, Department of Medicine, Memorial Sloan Kettering Cancer Center, New York, NY 10065, USA

ARTICLE INFO

Article history:
Received 10 July 2017
Received in revised form 14 November 2017
Accepted 16 November 2017
Available online 21 November 2017

Keywords:
STAT1
MPN
CDK8
Kinase inhibitor
Leukemia
Super-enhancer
Cortistatin A
Ruxolitinib

ABSTRACT

Constitutive JAK-STAT signaling drives the proliferation of most myeloproliferative neoplasms (MPN) and a subset of acute myeloid leukemia (AML), but persistence emerges with chronic exposure to JAK inhibitors. MPN and post-MPN AML are dependent on tyrosine phosphorylation of STATs, but the role of serine STAT1 phosphorylation remains unclear. We previously demonstrated that Mediator kinase inhibitor cortistatin A (CA) reduced proliferation of JAK2-mutant AML in vitro and in vivo and also suppressed CDK8-dependent phosphorylation of STAT1 at serine 727. Here we report that phosphorylation of STAT1 S727 promotes the proliferation of AML cells with JAK-STAT pathway activation. Inhibition of serine phosphorylation by CA promotes growth arrest and differentiation, inhibits colony formation in MPN patient samples and reduces allele burden in MPN mouse models. These results reveal that STAT1 pS727 regulates growth and differentiation in JAK-STAT activated neoplasms and suggest that Mediator kinase inhibition represents a therapeutic strategy to regulate JAK-STAT signaling.

1. Introduction

Myeloproliferative neoplasms (MPNs) are a class of hematopoietic disorders characterized by clonal proliferation of myeloid cells (Spivak, 2004). Up to 20% of MPN patients progress to acute myeloid leukemia (post-MPN AML) (Mesa and Tibes, 2012). Most MPN patients exhibit constitutive JAK-STAT signaling, often through an activating somatic mutation in kinase JAK2 (V617F) (Baxter, 2005; James et al., 2005; Kralovics et al., 2005; Levine et al., 2005; Zhao et al., 2005) or upstream in the thrombopoietin receptor MPL (W515 L/K) (Pikman et al., 2006; Pardanani et al., 2006). This leads to abnormal signaling through PI3K, ERK, and STATs (James et al., 2005; Lu et al., 2005; Lucet, 2006). Although MPN cells are known to rely on JAK2, STAT3 and STAT5 for survival and proliferation (Yan et al., 2012; Friedbichler et al., 2010; Walz et al., 2012; Funakoshi-Tago et al., 2010; Jedidi et al., 2009; Roder, 2001; Kleppe et al., 2015), the extent of their dependence on STAT1 remains unknown. Subsets of MPN patients have high levels of STAT1 signaling compared to healthy controls, and Stat1 was shown to be required in the *Jak2*V617F-knockin mouse model as well as to contribute to hyperproliferation in engineered *Jak2*V617F murine fetal liver progenitors (Chen et al., 2010; Jiahai Shi et al., 2016; Duek et al., 2014). Moreover, STAT1 has been shown to be activated in cycling hematopoietic stem cells (HSCs), raising the possibility that it controls stem-like programs (Knapp et al., 2017; Trumpp et al., 2010; Essers et al., 2009).

The JAK-STAT pathway is involved in cell growth, differentiation, apoptosis, and other integral cellular functions (Furqan et al., 2013; Vainchenker and Constantinescu, 2013; Ferrajoli et al., 2006). Aberrant STAT signaling has been documented in a variety of leukemias, including AML, chronic myelogenous leukemia (CML), and acute lymphoblastic leukemia (ALL) (Lin et al., 2000; Weber-Nordt et al., 1996). About half of AML patients have activated STAT1 signaling (Aronica et al., 1996; Gouilleux-gruart et al., 2009). In 2011, the JAK1/2 inhibitor ruxolitinib was approved as the first targeted therapy for myelofibrosis, a subset of MPN. Although ruxolitinib improves splenomegaly and constitutional symptoms in patients, the development of persistence remains an obstacle for long-term efficacy (Koppikar et al., 2012). Furthermore, adverse immunosuppressive effects of JAK inhibition

* Corresponding author.
E-mail address: shair@chemistry.harvard.edu (M.D. Shair).

https://doi.org/10.1016/j.ebiom.2017.11.013

have been reported in patients (Schonberg et al., 2015; Parampalli Yajnanarayana et al., 2015). Consequently, there is an unmet need for safe and synergistic combination therapies that can overcome these limitations. Additionally, patients with post-MPN AML are refractory to standard AML therapies, constituting a population that would especially benefit from new therapeutics (Mascarenhas et al., 2012).

JAKs phosphorylate STAT transcription factors on a tyrosine residue to induce STAT dimerization and nuclear translocation, which ultimately regulates transcription. In a less well-understood process, STAT transcriptional activity is also regulated by the Mediator-associated kinase CDK8. CDK8 (or its paralog CDK19) can associate with CCNC (cyclin C), MED12, and MED13 to form a CDK8 module that reversibly associates with Mediator, a large multisubunit complex that regulates transcription (Allen and Taatjes, 2015). CDK8 was reported to phosphorylate the transactivation domains (TADs) of STATs, suggesting that CDK8 inhibitors might modulate expression of STAT target genes and thereby inhibit the proliferation of JAK2-mutant cells that are resistant to JAK inhibitors (Bancerek et al., 2013). The marine natural product cortistatin A (CA, PubChem CID 11561907), a specific inhibitor (Cee et al., 2009) of CDK8 and CDK19 (collectively "Mediator kinases"), inhibits the proliferation of AML cell lines with a variety of oncogenic drivers, including JAK2(V617F), and is efficacious in in vivo models of AML (Pelish et al., 2015). Super-enhancers (SEs) are large stretches of regulatory DNA loaded with transcriptional regulators that drive high expression of cell identity and disease genes (Hnisz et al., 2013; Lovén et al., 2013). CA disproportionately increases transcription of SE-associated genes in sensitive AML cells, including those encoding transcription factors with tumor suppressor and lineage-controlling functions (Pelish et al., 2015).

Here we report that Mediator kinase inhibition with CA suppresses the growth of AML cells with hyper-activated JAK-STAT signaling in part by blocking STAT1 S727 phosphorylation. We also show that differentiation of these AML cells is mediated, in part, by CDK8 phosphorylation of STAT1 S727. CA acts through transcriptional and functional mechanisms distinct from those of ruxolitinib, which reduces STAT tyrosine phosphorylation. We found that STAT1 pS727 is loaded at SE-associated genes in these cells, many of which are upregulated upon Mediator kinase inhibition. Moreover, CA inhibits the growth of JAK-inhibitor persistent cells, suppresses colony formation in primary MPN patient samples, reduces allele burden in MPN mouse models, and demonstrates synergy with ruxolitinib.

2. Materials and Methods

2.1. Cell Culture

Cell line media: 6133-*MPLW515L* in RPMI-1640, 10% FBS; SET-2 in RPMI-1640, 20% FBS and SET-2^{Per} plus 0.7 μM ruxolitinib; UKE-1 in RPMI-1640, 10% FBS, 10% horse serum and 1 μM hydrocortisone and UKE-1^{Per} plus 1 μM ruxolitinib. All media was supplemented with 100 U/mL penicillin and 100 μg/mL streptomycin. UKE-1, UKE-1^{Per}, SET-2, and SET-2^{Per} were a kind gift from Ross Levine.

2.2. Growth Assays

All cells were plated (96-well) in triplicate at 10,000 to 20,000 cells/well for testing (n = 3). Cells were incubated in the presence of vehicle (0.1% DMSO) or specified compound. Viable cell number was estimated after 3, 7, and 10 days by counting viable cells from one vehicle well, generating a cell dilution series, transferring 20 μL/well in duplicate to a 384-well plate, and performing a linear regression to CellTiter-Glo (Promega) response (SPECTRAmax M3, Molecular Devices). Cells from all wells were also 4-fold diluted in media and transferred in duplicate for CellTiter-Glo measurement. On days 3 and 7, an equal volume for all wells were split-back with fresh media and compound, such that the resulting cell density for the vehicle well matched the initial seeding density. For days 7 and 10, estimated cell number represents the split-adjusted theoretical cell number. For growth assays with inhibitors, n = 3 for each concentration. At least two or three independent experiments were performed for each compound.

2.3. Colony Formation Unit Assays

Peripheral blood mononuclear cells from MPN patients were provided by the MSKCC Hematology Oncology Tissue Bank. CD34^{+} cells were isolated using the human CD34 MicroBead Kit (Miltenyl) and seeded in 10 mm dishes in duplicate in MethoCult treated either with 0.1% DMSO (vehicle), CA, or ruxolitinib, and CFU-GM colonies were counted at 14 days.

2.4. PBMC Viability and Western Blot Assay

A frozen PBMC stock from a single donor (Zen-Bio) was thawed and resuspended in RPMI supplemented with 10% heat inactivated FBS and viable cell number determined by hemocytometer at 95%. The PBMCs were then divided for viability testing and western blot analysis. In the viability test, PBMCs were dispensed into 4 × 96 w black walled clear-bottom plates at 30,000 cells per well for testing each treatment in triplicate. Also on each plate, PBMCs were seeded in a 2-fold dilution series from 120,000 cells to ensure a linear response at the viability measurement timepoint. After 16 h, vehicle (0.2% DMSO) or specified compounds were added to all wells (n = 3). After 24 h and 72 h, CellTiter-Blue (Promega) was added as specified by the manufacturer and fluorescence was recorded after 1 h, 3 h, 6 h, 24 h (SPECTRAmax M3, Molecular Devices). After background subtraction (wells with no cells), the cell number vs. response signal was examined and the initial seeding density of 30,000 cells was in the linear range for response at 6 h post-CellTiter-Blue addition. The data for this timepoint was normalized to vehicle for each plate and plotted using GraphPad Prism. Only one independent experiment was performed. For western blotting, PBMCs were seeded at 2 million per mL in 6 well plates. After 16 h, vehicle (0.2% DMSO) or specified compounds were added. After 4 h, media was removed and the cells were processed as described in the Western blotting section. PBMC were pelleted, washed with PBS, and resuspended in lysis buffer (CST) containing 150 mM NaCl, 20 mM Tris-HCl (pH 7.5), 1% Triton X-100, 1 mM Na2EDTA, 1 mM EGTA, 2.5 mM sodium pyrophosphate, 1 mM beta-glycerophosphate, 1 mM Na3VO4, 1 μg/mL leupeptin, supplemented with 1× HALT protease/phosphatase inhibitors cocktail (Thermo Fisher), 2 mM PMSF (G Biosciences), and 1 mM 3,4-dichloroisocoumarin (Sigma).

2.5. In Vivo MPN Model

Bone marrow from primary CD45.2 *Jak2*V617F mice was mixed 1:1 with CD45.1 C57BL/6 marrow and transplanted into lethally irradiated CD45.1 C57BL/6 recipients (Mullally et al., 2010). Peripheral blood counts were measured to verify disease establishment and for randomization into treatment groups. Treatment with CA at 0.16 mg/kg per day was compared to ruxolitinib at 60 mg/kg twice daily or vehicle over 4 weeks. Spleen weights were assessed at time of sacrifice. Mutant allele burden was determined as the fraction of CD45.2 bone marrow cells. Animal care was in strict compliance with institutional guidelines established by Memorial Sloan Kettering Cancer Center, the Guide for Care and Use of Laboratory animals and the Association for Assessment and Accreditation of Laboratory Animal Care International.

2.6. Synergy Experiments

SET-2 and UKE-1 cells were co-treated with constant ratios of ruxolitinib (ChemTek) to CA, 1 to 1 or 10 to 1, in a 96-well growth

assay format with a range of 2-fold dose dilutions of compounds in triplicate (see growth assay method using CellTiterGlo). SET-2 and UKE-1 cells were also treated with ruxolitinib alone or CA alone in a 2-fold dilution series in triplicate. The Chou-Talalay combination index values at 50% growth inhibition ($F_a = 0.5$) were determined using CalcuSyn software (Chou, 2010). Experiments were repeated independently at least four times.

2.7. Competitive Growth Assays

For competitive growth assays with two cell lines, each cell line was plated (96-well) in triplicate at 10,000/well for testing, for a total of 20,000 cells/well. At this time (day 0), aliquots of each combination were taken for flow cytometric analysis and the actual starting ratio of cell line A to cell line B was calculated by dividing the fraction of mCherry-positive events by the fraction of ZsGreen-positive events (or vice-versa, depending on the experimental comparison). Cells were then incubated in the presence of vehicle, CA, ruxolitinib, taxol (LC Laboratories), or doxorubicin (Sigma-Aldrich). Cell line ratios were determined at days 4, 8, and 12 by taking aliquots of cells, transferring to 96-well V-bottom plates, and running them through the flow cytometer using the HTS plate reader instrument on the BD Fortessa. Just as for Day 0, the ratios were calculated by measuring fractions of mCherry vs. ZsGreen events. At days 4 and 8, an equal volume for all wells were split-back with fresh media and compound, such that the resulting cell density for the vehicle well matched the initial seeding density.

2.8. Western Blotting and Immunoprecipitation

Cells were treated with CA, ruxolitinib, or DMSO for 2 h. Pellets were collected and washed with PBS, then lysed with RIPA buffer (Sigma R0278) supplemented with protease inhibitors (Sigma P8340) and phosphatase inhibitors (Sigma P0044 and P5726). Proteins were resolved on NuPAGE 4–12% polyacrylamide gels in LDS buffer (Thermo Fisher), transferred to PVDF membranes with Tris-Glycine transfer buffer, blocked with 5% BSA or 5% milk in 0.1% TBST, then probed with antibodies. Primary antibodies included: STAT1 (CST #9172), STAT1 (R&D Systems #PAF-ST1), STAT1 pS727 (CST #9177), STAT1 pY701 (CST #9167), CDK8 (CST #4101 or #4106), CDK19 (Sigma #HPA007053), CDK9 (CST #2316), FLAG (Sigma F1804), PARP (CST #9532), actin (Sigma #A5060), GAPDH (Santa Cruz sc-47724). For secondary antibodies, we used either anti-rabbit IgG HRP conjugate (Promega #401B) or anti-mouse IgG HRP conjugate (Promega #402B).

2.9. Plasmids

pLVX-EF1a-CDK8-W105M-mCherry and pLVX-EF1a-CDK8-WT-ZsGreen were prepared as previously described (Pelish et al., 2015). STAT1 WT (Addgene #12301) was FLAG-tagged and cloned into pLVX-EF1alpha-IRES-mCherry, STAT1 S727E (Addgene #12305) or STAT1 S727A (Addgene #12304) were FLAG-tagged and cloned into pLVX-EF1alpha-IRES-ZsGreen (Clontech) and transformed into *E. coli* (Stellar Competent Cells, Takara). The lentiCas9-Blast (Addgene #52962) plasmid was modified into the Cas9-P2A-ZsGreen-Blast plasmid by cloning in a P2A-ZsGreen sequence generated from the pLVX-IRES-ZsGreen vector. Vector pLKO.1-TagFP635-puro (Sigma) was used to generate pLKO.1-AmCyan-puro by cloning in AmCyan (Takara #632440). For sgRNA plasmids, DNA oligonucleotides (IDT) corresponding to the sgRNA sequence were annealed into oligo duplexes and cloned into an inserted PsrI site located in the FP635 vector or the AmCyan vector. pLVX or pLKO.1 lentiviral vectors were co-transfected with psPASx and pMD2.G (Addgene) in 293 T cells. After 48 h, viral supernatants were collected and passed through a 0.45 μm filter (Millipore). For transductions, 24-well plates were coated with 500 μL of 20 μg/mL RetroNectin (Takara) at 4 °C overnight, blocked with 2% BSA for 30 min, washed with PBS, and 300–500 μL of viral supernatant was added. The plates were centrifuged (2000 g, 1.5 h) and then set in an incubator. After 2 h, viral supernatant was removed and 500 μL/well of 200,000 cells/mL was added. After 3 days, the cells were expanded and isolated by FACS.

2.10. Native Kinase Capture

Experiments were performed as previously described (Pelish et al., 2015). 5×10^8 SET-2 cells were washed twice with 10 mL cold PBS and resuspended in 1 mL cold kinase buffer (20 mM HEPES, pH 7.4, 150 mM NaCl, 0.5% Triton X-100, with inhibitors 11,697,498,001, Roche and P5726, Sigma). Cells were lysed by sonication (2 × 10 s pulses with a 30 s break) and centrifuged (16,000 *g*, 10 min). The supernatant was desalted through a column (732–2010, Biorad) and the eluted lysate was diluted to 5 mg mL^{-1} with kinase buffer. For each treatment, 475 μL of the lysate was pre-incubated with 10 μL MnCl2 (1 M) and 5 μL compound to the desired concentration at room temperature for 30 min. Uninhibited kinases were captured with 10 μL ActivX desthiobiotin-ATP probe (0.25 mM; 88,311, Pierce) at room temperature for 10 min. Samples were mixed with 500 μL urea (8 M; 818,710, Millipore) and 50 μL streptavidin agarose (20,359, Thermo) for 60 min at room temperature on a nutator. Beads were washed twice with a 1:1 mixture of kinase buffer and 8 M urea, and collected by centrifugation (1000 *g*, 1 min). Proteins were eluted from the beads with 100 μL 2 × LDS sample buffer (NP0007, Life) at 95 °C for 10 min. Samples were analysed by standard immunoblotting and horseradish peroxidase detection. Experiment was performed twice.

2.11. ddPCR

Total RNA was isolated from 10^6 SET-2 cells (RNeasy Plus Mini Kit, Qiagen) and quantified by Nanodrop. Total RNA was reverse-transcribed into cDNA (High Capacity cDNA Reverse Transcriptase Kit, Applied Biosystems) and used (ddPCR Supermix for Probes, no dUTP, Bio-Rad 186-3024) with TaqMan FAM probes for genes of interest and ACTB (VIC) as the reference gene. Droplets were generated in the QX200 Droplet Generator, thermocycled, and read on the QX200 Droplet Reader. Probes used (Life Technologies): CD41 (Hs01116228_m1), CD61 (Hs01001469_m1), GATA1 (Hs0185823_m1), GATA2 (Hs00231119_m1), ID2 (Hs04187239_m1), UBASH3B (Hs00262721_m1), MEF2C (Hs00231149_m1), ZEB2 (Hs00207691_m1), VEGFA (Hs00900055_m1), BMPER (Hs00403062_m1), ACTB (4325788); and custom-ordered from IDT: BCL3 (probe/56-FAM/ACG TCA GCA/ZEN/CCC GTC ACT CA/3IABkFQ/; Rev. Primer GGG TTA AGG TTG GAG GAA GC, For. Primer AGA ACT TGA CCG CAA CCC), JAK2 (probe/56-FAM/CGG CGT TGA/ZEN/GAA GAC GGT GT/3IABkFQ/, Rev. Primer ACA GTT GTC TCC ACC CTC TC, For Primer AAC CGG GAG GCT GAG TT), IRF1 (probe/56-FAM/AAG TGT TTG/ZEN/GAT TGC TCG GTG GC/3IABkFQ/, Rev. Primer CGA AAT GAC GGC ACG CA, For. Primer TCT TGC CTC GAC TAA GGA GTG), STAT1 (probe/56-FAM/CGC TGG GAA/ZEN/CTG GCG TTC TGT TTA/3IABkFQ/, Rev. Primer CAC GTC CTT CTG ATC GTT CTC, For. Primer TAT TTC CGC CGG CTT CC), RABA4 (probe/5HEX/ACT GGC ATT/ZEN/TTC CAC ACA GTC CAG GT/3IABkFQ/, For. Primer CTT GGC TAA GCT CCC AAG TG, Rev. Primer GAG GAT GGA GCC AAA CTG AC).

2.12. Flow Cytometry

Cells were plated (6-well) in triplicate at 150,000 cells/mL for 3-day timepoints. For the 6-day timepoint, cells were plated at 35,000 cells/mL and diluted to 150,000 cells/mL with media and compound on day 4. For cell cycle, cells were washed twice with PBS, fixed with 70% ethanol at 4 °C overnight, washed with PBS, and stained with 50 μg/mL propidium iodide (eBioscience) for 1 h at 37 °C. For apoptosis, cells

were stained using Annexin V-FITC (BD Pharmingen) and 7-AAD (Miltenyi Biotec). Samples were acquired on a BD LSR II or BD Fortessa and analysed using FlowJo v7.6.5. For differentiation, cells were stained with anti-CD41-PerCP (Abcam ab134373) or anti-CD61-PE (Abcam ab91128) for SET-2 cells or CD41-PEcy7 (eBioscience 25-0411-82) or CD42-PE (Emfret M040-2) for 6133/MPL cells. For each experiment, n = 3 biological replicates with two independent experiments and one shown.

2.13. ChIP-seq

Untreated cells or cells treated with CA (25 nM, 4 h) or vehicle were crosslinked for 10 min at room temperature by addition of one-tenth of the volume of formaldehyde solution (11% formaldehyde, 50 mM HEPES pH 7.4, 100 mM NaCl, 1 mM EDTA, 0.5 mM EGTA) to the media followed by 5 min quenching with 125 mM glycine. ChIP was performed as previously described (Pelish et al., 2015), with modifications. All subsequent buffers were supplemented with protease inhibitor tablets (Roche #05056489001) and, for phosphospecific ChIP-seq, phosphatase inhibitor tablets (Roche #4906845001). Briefly, cells were lysed with lysis buffer 1 (50 mM HEPES pH 7.4, 140 mM NaCl, 1 mM EDTA, 10% glycerol, 0.5% NP-40, and 25% Triton X-100) and washed with lysis buffer 2 (10 mM Tris-HCl pH 8.0, 200 mM NaCl, 1 mM EDTA, and 0.5 mM EGTA). The nuclei were resuspended in TF sonication buffer (300 mM NaCl, 10 mM Tris-HCl pH 8.0, 1 mM EDTA pH 8.0, 0.1% Na-Deoxycholate, 0.1% SDS, 1% Triton X-100, 0.25% Sarkosyl), then sheared for 4 min (STAT1, STAT1 pS727) (pulse, 0.7 s on, 1.3 s off, 10–12 watts) on wet ice. Sonicated lysates were cleared and incubated overnight at 4 °C with Protein G magnetic Dynal beads pre-bound with the indicated antibodies. For ChIP or ChIP-seq, antibodies included Normal Rabbit IgG (CST #2729), STAT1 pS727 (Life Tech #44-382G) or STAT1α/β (Santa Cruz sc-346). For STAT1 ChIP-seq, for each treatment group, three sets of 3.3×10^7 cells were independently pulled down with 15 μg of antibody, then pooled into 2 replicates at the library prep stage. For phospho-specific STAT1 ChIP-seq, four sets of 10^8 cells were lysed and pulled down with 40uL of antibody, then pooled at the library prep stage into 2 replicates. Beads were washed with sonication buffer, sonication buffer with 500 mM NaCl, LiCl wash buffer (20 mM Tris-HCl pH 8.0, 1 mM EDTA, 250 mM LiCl, 0.5% NP-40, 0.5% sodium deoxycholate) and TE. Bound complexes were eluted with 50 mM Tris-HCl pH 8.0, 10 mM EDTA, 1% SDS at 65 °C and reverse crosslinked at 65 °C. RNA and protein were digested using RNAse A and proteinase K, respectively, and DNA was purified using Qiagen MinElute columns. Libraries were prepared using the KAPA Hyper Prep Kit for Illumina and ligated to unique Bioo Scientific NEXTflex barcode adaptors. Following ligation, libraries were amplified with 16–18 cycles of PCR and were then size-selected using a 2% gel cassette in the Pippin Prep System from Sage Science. For transcription factors, DNA fragments of size 200-500 bp were captured. Libraries were quantified by qPCR utilizing the KAPA Biosystems Illumina Library Quantification kit. Libraries with distinct indexes were then combined in equimolar ratios and run together in a lane on the Illumina HiSeq 2500 or NextSeq 500 for 50 or 75 bases in single read mode. Next-generation sequencing data were stored in NCBI's public repository Gene Expression Omnibus (GEO) under accession number GSE100566.

2.14. Analysis of ChIP-seq Data

We have previously published CDK8 and H3K27ac ChIP-seq data in SET-2 cells (Pelish et al., 2015). STAT1 and STAT1 pS727 ChIP-seq data sets were aligned using Bowtie (v1.1.1) (Langmead et al., 2009) to build version NCBI37/HG19 of the human genome (-n 1 -m 1 –best –strata). We used the MACS2 (Zhang et al., 2008) peak-finding algorithm (standard parameters) to identify enriched ChIP-seq regions over inputs. Reproducibility of each independent STAT1 and STAT1 pS727 ChIP-seq experiment was assessed according to the pipeline developed for the ENCODE project (https://sites.google.com/site/anshulkundaje/projects/idr) (Li et al., 2011). IDR was determined as recommended on peaks called by SPP (Kharchenko et al., 2008) at FDR < 0.5. Duplicate reads were removed using Picard tools (version 1.88). Regions of interest were retained, merged and annotated by overlap with RefSeq genes (genomic coordinates downloaded from UCSC refgene table Apr. 26, 2013) using *bedtools* (Quinlan and Hall, 2010) or HOMER (Heinz et al., 2010). Retained regions were assigned to one of the following categories: (1) promoter = TSS-500 bp to TSS + 200 bp, (2) body = TSS + 201 bp to TES, (3) 5′ UTR = TSS-10 kb to TSS-501 bp, and (4) 3′ UTR = TES + 1 bp to TES + 10 kb. All other regions were termed "desert" hits. Any gene satisfying the overlap criteria was included in the corresponding category. Transcripts sharing identical TSS and TES coordinates were represented a single time in the count statistics. For assignment of top 500 STAT1 pS727 enhancers, STAT1 pS727 regions were ranked by MACS2 peakscore, peaks in proximity to the TSS (−1 kb to +100 bp) were excluded, and the top 500 remaining regions corresponding to unique genes were selected for GSEA against the RNA-seq DE gene list (resulting in a filtered list of 439 genes). Analysis of Motif Enrichment (AME, MEME Suite) was performed by extracting FASTA sequences of 500 bp centered regions from STAT1 and STAT1 pS727 bed files. Tracks shown in Fig. 5C were obtained by conversion of bedGraph files (normalized to reads per million (RPM) using macs2 -B – SPMR) to bigWig format and were visualized using Integrative Genomics Viewer.

2.15. RNA-seq Data Analysis

Our RNA-seq data in SET-2 cells treated with CA or DMSO for 4 h was previously published and can be accessed from GSE65161. Normalized counts matrices from RNA-seq data of SET-2 cells treated with ruxolitinib or DMSO were downloaded from GSE69827 and differentially expressed genes were extracted using Degust (http://www.vicbioinformatics.com/degust/index.html), which uses limma and edgeR to generate $\log_2$ fold change and FDR-q values. Without any FDR-q or p-value cutoffs, we determined the overlap of the two RNA-seq datasets by Gene Symbol (n = 17,814), then generated the scatterplot of DE genes with ruxolitinib vs. CA using ggplot in R (version 3.2.3). Gene Set Enrichment Analysis (GSEA (Mootha et al., 2003; Subramanian et al., 2005) version 1) was run with rank-ordered DE gene lists for CA or ruxolitinib treatment. The signatures used for GSEA included: TENEDINI_MEGAKARYOCYTE_MARKERS (MSigDB), HaemAtlas MK-specific gene set (extracted from ArrayExpress accession E-TABM-633) (Watkins et al., 2009), and CFU-MK and MK specific gene set (extracted from GEO accession GSE24759) (Novershtern et al., 2011) Gene lists were submitted to DAVID (http://david.abcc.ncifcrf.gov) for functional annotation/gene ontology analysis (Huang et al., 2008).

2.16. CRISPR-Cas9 Editing

Cells were transduced with Cas9, purified by FACS, and selected with blasticidin for 1 week (Thermo Fisher) to generate stably-expressing cells. For knockouts, Cas9-cells were then transduced with pLKO.1-sgSTAT1-FP635 (guides #1, 3, 2n, 9n, 4, 11) or pLKO.1-sgAAVS1-AmCyan. For knockin of STAT1 S727E, Cas9-cells were transduced with pLKO.1-sgSTAT1-FP635 (guide sg9) and immediately nucleofected (Amaxa Nucleofector IIb and Ingenio electroporation solution) with a 160-bp repair oligonucleotide containing the STAT1 S727E mutation (IDT Ultramer.). After 3–7 days, cells were purified by FACS. After 10 days or 16 days, aliquots of cells were processed to extract genomic DNA (Qiagen DNeasy Blood and Tissue Kit), PCR amplify a 200 bp region around the mutation site, and acquire next-generation sequencing data (CCIB MGH DNA Core). FASTQ files were analysed using CRISPResso (Pinello et al., 2016). Single cell clones were sorted by FACS in 96-well plates and grown to confluency. Aliquots of cells were transferred to fresh V-bottom plates, washed with PBS, and lysed using QuickExtract buffer (EpiBio). Genomic DNA from the extracts was used to amplify a 1 kb region around S727 by PCR and sent for Sanger sequencing. The

CRISP-ID online platform was used to identify indels in single-cell clones (http://crispid.gbiomed.kuleuven.be) (Dehairs et al., 2016). Sequences for guide RNAs: sgAAVS1 (CGATGCACACTGGGAAG); for STAT1: sg1 (TTCCCTATAGGATGTCTCAG), sg3 (CATGGAAATCAGACAGTACC), sg2n (GAGGTCATGAAAACGGATGG), STAT1-9n (GATCATCCAGCTGTGACAGG), sg4 (AGGAGTTTGACGAGGTGTCT), sg5 (GACACCTCGTCAAACTCCTC), sg9 (CAAACTCCTCAGGAGACATG), sg11 (GTCAAACTCCTCAGGAGACA).

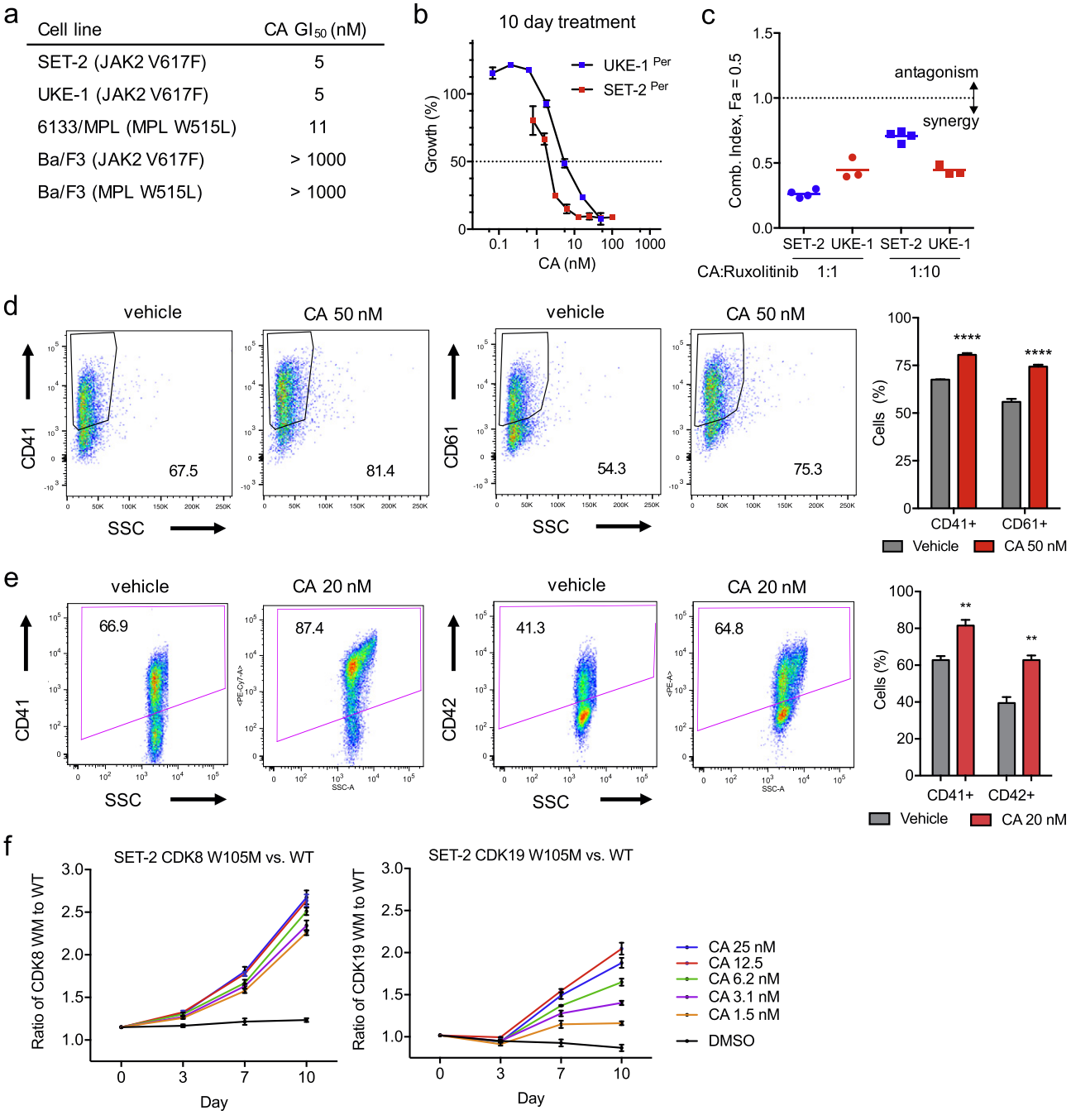

Fig. 1. Inhibition of CDK8/CDK19 reduces proliferation and promotes differentiation of JAK-STAT activated AML and AMKL. A. JAK2-dependent AML cell lines SET-2 and UKE-1, and AMKL cell line 6133/MPL are highly sensitive to CDK8/19 inhibition by cortistatin A (CA). Ba/F3 pro-B cells expressing *JAK2 V617F* or *MPL W515L* are resistant to CA. Doses of CA causing 50% growth inhibition (GI_{50}) calculated from full-dose response curves from at least three separate experiments with three biological replicates per dose. B. Ruxolitinib-persistent cell lines SET-2^{Per} and UKE-1^{Per} retain sensitivity to CA (mean ± s.e.m. of n = 3 biological replicates). Representative growth curves shown for experiments repeated at least three times. C. CA and ruxolitinib show synergy in SET-2 and UKE-1 cells. Cells were treated with CA alone, ruxolitinib alone, and CA and ruxolitinib in 1:1 or 1:10 ratios for 10 days and combination index values were assessed at 50% growth. Each dot represents one full independent experiment in which synergy was assessed. D. CA promotes megakaryocytic differentiation in SET-2 cells after 3 days of treatment. Representative flow cytometry traces shown. Quantification of mean ± s.e.m., n = 3 biological replicates, one of two independent experiments shown. E. CA induces dose-dependent upregulation of the megakaryocyte markers CD41 and CD42 in 6133/MPL cells after 7 days of treatment. Representative flow cytometry traces shown. Quantification of mean ± s.e.m., n = 3 biological replicates, one of two independent experiments shown. F. Competitive growth assays show that SET-2 cells overexpressing CA-resistant CDK8 W105 M or CDK19 W105 M (mCherry) outcompete cells expressing wild-type CDK8 or CDK19 (ZsGreen) in the presence of CA, respectively (mean ± s.e.m. ratio of n = 3 biological replicates). Representative growth curves shown for experiments repeated at least three times. See also Fig. S1. For all figures, *P < 0.05 **P < 0.01 ***P < 0.001 ****P < 0.0001 or ns (not significant).

3. Results

3.1. CDK8/CDK19 Inhibition Reduces Growth and Promotes Differentiation of JAK-STAT Activated AML Cells

We reported that post-MPN AML cell lines SET-2 and UKE-1 are sensitive to CDK8/19 inhibition with CA (GI_{50} = 5 nM, 10-day growth assay; Fig. 1A) (Pelish et al., 2015). SET-2 and UKE-1 cells are derived from patients with essential thrombocythemia (ET), a *JAK2 V617F*-mutant MPN, that progressed to AML. To investigate whether JAK-STAT activated cells are generally sensitive to CDK8/19 inhibitors, we tested other cell lines with constitutively activated JAK-STAT signaling. Murine 6133/MPL cells, an acute megakaryoblastic leukemia (AMKL) cell line with the JAK-STAT-activating mutation *MPL W515L*, were also sensitive to CA (GI_{50} = 11 nM, 10-day growth assay; Fig. 1A). Notably, murine Ba/F3 cells expressing either *JAK2 V617F* or *MPL W515L*, which confer cytokine-independent growth, are sensitive to ruxolitinib (Quintas-Cardama et al., 2010) but not to CA (GI_{50} > 1000 nM, 10-day growth assay; Fig. 1A). We previously determined that the HEL cell line, an erythroleukemia cell line which also carries the *JAK2 V617F* mutation, is insensitive to CA (Pelish et al., 2015). Ruxolitinib only partially inhibits the proliferation of HEL cells, suggesting that this cell line might not be completely JAK2-dependent and therefore a flawed model of JAK2-activated neoplasms (Quintas-Cardama et al., 2010). Taken together, however, HEL and Ba/F3 *JAK2 V617F* insensitivity to CA point to the possibility that CDK8 activity is largely context-dependent in JAK2-activated neoplasms. SET-2, UKE-1, and 6133/MPL are myeloid cells whereas Ba/F3 are lymphoid pro-B cells and HEL are erythroid cells, indicating a role for cell lineage in conferring sensitivity to CA but not to ruxolitinib and revealing underlying mechanistic differences between Mediator kinase inhibition and JAK1/2 inhibition.

A challenge associated with chronic JAK1/2 inhibition is the emergence of persistence, resulting in reactivated JAK-STAT signaling and proliferation (Koppikar et al., 2012). We therefore tested CA in AML cells that had become persistent to JAK2 inhibition after long-term treatment with ruxolitinib (SET-2^{Per}, UKE-1^{Per}, Fig. 1B). These persistent cell lines retained their sensitivity to CA treatment (SET-2^{Per} GI_{50} = 2 nM; UKE-1^{Per} GI_{50} = 5 nM), suggesting that CDK8/19 inhibition bypasses JAK1/2 persistence mechanisms. Given this result, we tested for anti-proliferative additivity or synergy between ruxolitinib and CA. The compounds synergistically inhibited the growth of SET-2 and UKE-1 cells at two different dose ratios (Chou-Talalay combination index (CI) values at 50% growth inhibition < 1, Fig. 1C). Therefore, Mediator kinase inhibitors offer the possibility to increase the effectiveness of JAK inhibitors for AML patients with constitutively activated JAK-STAT signaling.

We sought to characterize the anti-proliferative mechanisms of CA by assessing effects on differentiation, cell cycle, and induction of apoptosis. In SET-2 megakaryoblastic cells, CA upregulated mRNA expression (Fig. S1A) as well as surface levels (Fig. 1D) of megakaryocytic-specific markers CD41 and CD61 (Pelish et al., 2015). In contrast, ruxolitinib treatment did not affect these differentiation markers in SET-2 cells (Fig. S1B), as has been reported by others (Wen et al., 2015). CA also induced an increase in surface expression of mature megakaryocytic markers CD41 and CD42 in megakaryoblastic cell line 6133/MPL (Fig. 1E). These results suggest that CA induces megakaryocytic differentiation in cells that are predisposed towards that lineage program. CA caused limited induction of apoptosis in SET-2, UKE-1, and SET-2^{Per} cells (Fig. S1C-E and Pelish et al., 2015), as well as modest increases in S-phase with concomitant decreases in G0/G1 phase in UKE-1 and SET-2 cells (Fig. S1C, D). These results suggest that CA induces a cell-type specific combination of growth arrest, apoptosis, and/or differentiation in AML cells, as we have previously reported (Pelish et al., 2015). This contrasts with the mechanism of action of ruxolitinib, which is cytotoxic to JAK-STAT activated cells (Quintas-Cardama et al., 2010; Wen et al., 2015).

To confirm that CDK8/19 inhibition mediates the observed anti-proliferative effects of CA, we transduced cells with CA-resistant point mutants *CDK8*(*W105M*) or *CDK19*(*W105M*) expressing mCherry or wild-type CDK8 or CDK19 expressing ZsGreen (controls) and grew them together in the presence of CA or vehicle. By flow cytometry, we observed that the ratio of mutants to wild-type cells increased over time in the presence of CA in a dose-dependent manner (Fig. 1F and Fig. S1F–H). We also confirmed that CA selectively inhibits CDK8 and CDK19 over similar transcriptional kinases like CDK9 in native kinase capture assays (Patricelli et al., 2011) using SET-2 cell lysates (Fig. S1I). Taken together, these results indicate that Mediator kinase inhibition promotes growth arrest and megakaryocytic differentiation, acts in synergy with JAK inhibition, and is able to bypass persistence in JAK-STAT activated AML cells.

3.2. CA Suppresses Growth of JAK2-Mutant AML Cells in Part by Inhibiting Phosphorylation of the STAT1 TAD

Differential STAT1 signaling has been previously implicated in abnormal differentiation phenotypes seen in MPN subtypes ET and polycythemia vera (PV), as well as hyperproliferation of erythroid progenitors in engineered murine *JAK2*V617F cells (Chen et al., 2010; Jiahai Shi et al., 2016). To compare the effects of Mediator kinase inhibition and JAK1/2 inhibition on STAT1, we treated SET-2 and UKE-1 cells with CA or ruxolitinib and performed immunoblotting for phosphorylated and total levels of STAT1 (Fig. 2A and Fig. S2A, B). CA potently and dose-dependently inhibited phosphorylation of STAT1 S727, while JAK inhibitor ruxolitinib inhibited phosphorylation of STAT1 Y701. Ruxolitinib did not affect STAT1 S727 phosphorylation, revealing that this mark can be decoupled from STAT1 Y701 phosphorylation. Co-treatment of cells with ruxolitinib and CA resulted in inhibition of both STAT1 pS727 and STAT1 pY701.

The anti-proliferative effects of STAT tyrosine phosphorylation inhibition have been well-documented using ruxolitinib and other JAK inhibitors (Fridman et al., 2010; Verstovsek and Kantarjian, 2007; Koppikar et al., 2010). However, the effects of inhibiting serine phosphorylation in the TAD have not been well described, and they seem to be cell type- and context-dependent (Qin et al., 2008; Putz et al., 2013; Bancerek et al., 2013; Decker and Kovarik, 2000; Timofeeva et al., 2006; Friedbichler et al., 2010). Since CA strongly inhibited CDK8-dependent STAT1 phosphorylation, we hypothesized that JAK-STAT activated AML cells might be dependent on STAT1 pS727 for maximal growth. To determine whether some of the anti-proliferative effects of CDK8/19 inhibition are exerted specifically through ablation of STAT1 pS727, we performed a competitive growth assay with cells overexpressing either phosphomimetic STAT1 S727E (ZsGreen) or wild-type STAT1 (mCherry). The S727E mutation mimics a constitutively phosphorylated state that cannot be blocked by CDK8/19 inhibition with CA. We observed that the ratio of mutant to wild-type cells increased over time in a CA-dose dependent manner (Fig. 2B and Fig. S2C). This effect was specific to CA-treated cells; treatment with control cytotoxic compounds paclitaxel or doxorubicin did not induce a competitive growth advantage to STAT1 S727E-expressing cells (Fig. S2D). Furthermore, overexpression of STAT1 S727E did not broadly render AML cells with different oncogenic drivers resistant to CA, such as SKNO-1 (AML1-ETO) or MV4;11 (MLL-AF4) cells (Fig. S2E).

To study the effects of endogenously expressed STAT1 S727E, we used CRISPR-Cas9 to knock in the *S727E* mutation at the *STAT1* locus in SET-2 cells. We isolated a homozygous single-cell clone that had been edited by microhomology-directed end-joining to express the *S727E* mutation in-frame (Fig. S3A). This clone was almost 40-fold more resistant to CA than a control cell line expressing a single-guide RNA (sgRNA) targeting the safe-harbor *AAVS1* locus (Figs. 2C and S3B), supporting a role for phosphorylation of STAT1 S727 in these JAK2-mutant AML cells.

STAT1 signaling has been implicated in megakaryopoiesis in mice and in *JAKV617F* MPN (Z. Huang et al., 2007; Duek et al., 2014; Chen et

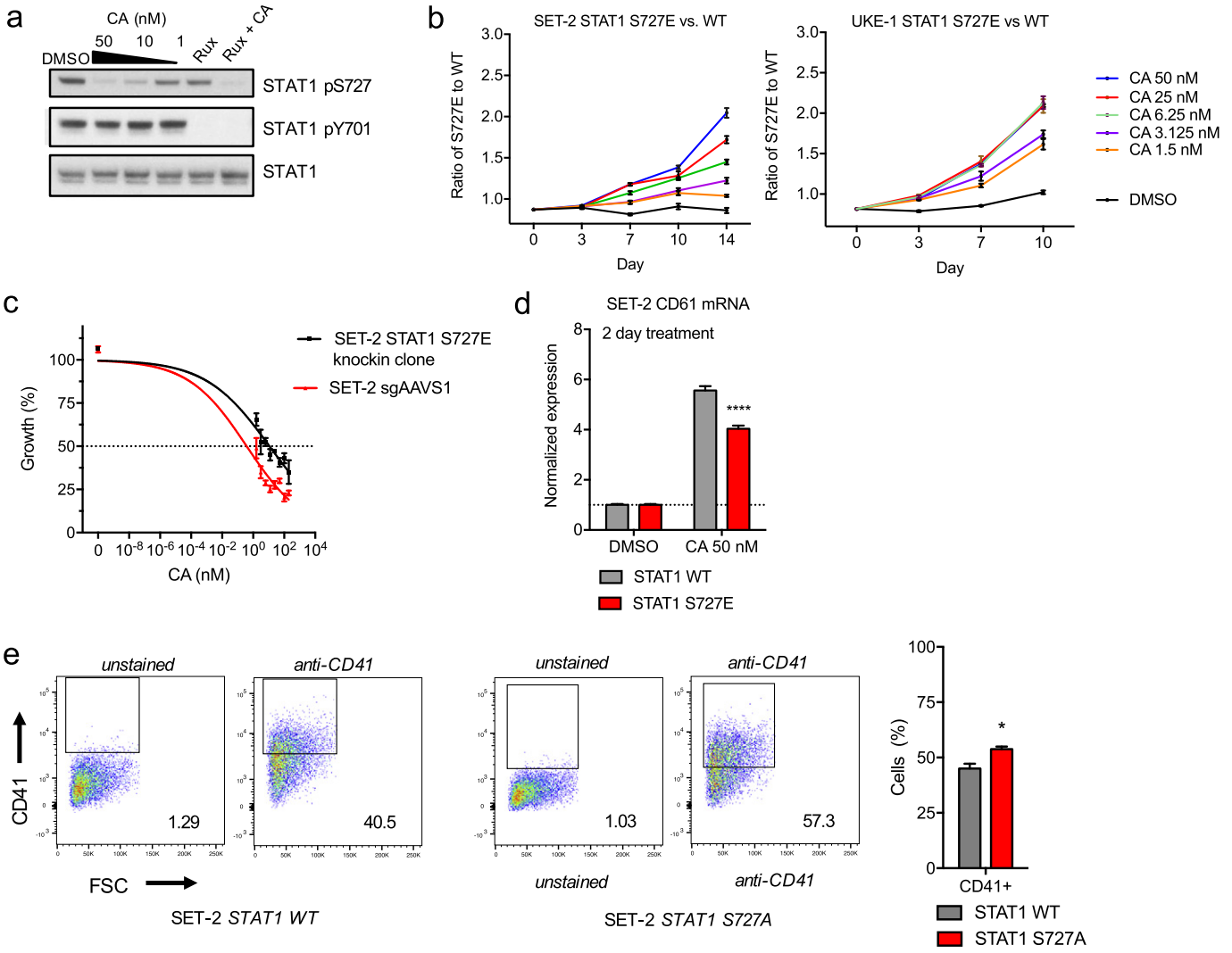

Fig. 2. CA suppresses growth of JAK2-mutant AML by inhibiting phosphorylation of STAT1 S727. A. Immunoblots after 2 h treatment showing dose-dependent inhibition of STAT1 S727 phosphorylation by CA in SET-2 cells. Ruxolitinib (Rux), a JAK1/2 inhibitor, inhibits tyrosine phosphorylation of STAT1 at 1 μm. Combined treatment with 1 μm ruxolitinib and 50 nM CA. Representative blots shown of at least three biological replicates. B. Competitive growth experiments show that SET-2 and UKE-1 cells overexpressing the phosphomimetic mutant STAT1 S727E (ZsGreen) outcompete cells expressing wild-type STAT1 (mCherry) in the presence of CA (mean ± s.e.m. ratio, n = 3 biological replicates). Representative growth curves shown for experiments repeated at least three times. C. A homozygous CRISPR-Cas9-edited clone expressing *STAT1 S727E* is resistant to CA compared to a control CRISPR knockout line targeting AAVS1. Solid lines represent calculated non-linear fit (STAT1 S727E(GI_{50}) = 37 nM, sgAAVS1(GI_{50}) = 0.3 nM). Dots represent the mean ± s.e.m. ratio of n = 3 biological replicates. D. CA-induced upregulation of CD61 can be inhibited by STAT1 S727E overexpression. CD61 mRNA transcript levels were measured by ddPCR (mean ± Poisson error, n = 5 biological replicates, experiment performed twice, P = 0.000091, two-tailed *t*-test). E. STAT1 S727A overexpression causes upregulation of CD41 on the cell surface compared to wild-type STAT1 in SET-2 cells. Representative flow cytometry traces shown and quantification plotted on the right (mean ± s.e.m., n = 4 biological replicates). See also Fig. S2.

al., 2010). We found that STAT1 serine phosphorylation regulates megakaryocytic differentiation in AML cells. Overexpression of mutant STAT1 S727E partially attenuated CA-induced upregulation of differentiation marker CD61 mRNA in SET-2 cells (Fig. 2D), but had no effect on CD41 mRNA (Fig. S3C). Overexpression of phospho-deficient mutant STAT1 S727A, which mimics the effects of CA on STAT1 phosphorylation, modestly promoted CD41 expression on the cell surface in SET-2 cells (Fig. 2E and Fig. S3D). These results reveal a dependence of JAK2-mutant AML cells on STAT1 pS727 for survival, proliferation, and differentiation.

3.3. Depletion of STAT1α or the TAD of STAT1 Induces Growth Arrest in JAK2-Mutant AML Cells

We hypothesized that if STAT1 were required for CA to suppress the growth of JAK2-mutant AML cells, knockout of STAT1 should render the cells resistant to CDK8 inhibition. There are two isoforms of STAT1 expressed in most cells, STAT1α (containing the TAD) and STAT1β (a splice variant lacking the TAD). We thus designed two CRISPR-Cas9 sgRNAs targeting exonic regions common to both isoforms, STAT1-sg9n and STAT1-sg1 (Fig. 3A). We knocked out STAT1 in SET-2 cells stably expressing Cas9 using sg9n or sg1 (co-expressing FP635) and measured their growth in culture in the presence of CA or vehicle in a two-color competitive growth format against control cells transduced with a sgRNA targeting safe harbor locus AAVS1 (co-expressing AmCyan). Knockout of STAT1 did not have a significant effect on growth response to ruxolitinib or doxorubicin, but it desensitized JAK2-mutant AML cells to CA (Fig. 3B and Fig. S4A, B). These results further support the hypothesis that STAT1 is a downstream effector of the anti-proliferative effect of CDK8/19 inhibition in these cells.

Total STAT1 knockout did not perturb basal growth (Fig. 3B, blue lines), suggesting that proliferation of JAK2-mutant AML could be regulated separately by STAT1α or STAT1β. The role of the TAD of STAT1, which includes residue serine-727, remains unclear, but it has been implicated in enhancing transcription of interferon-inducible genes (Bancerek et al., 2013; Decker and Kovarik, 2000). To isolate the function of the TAD in maintaining cell growth, we performed selective

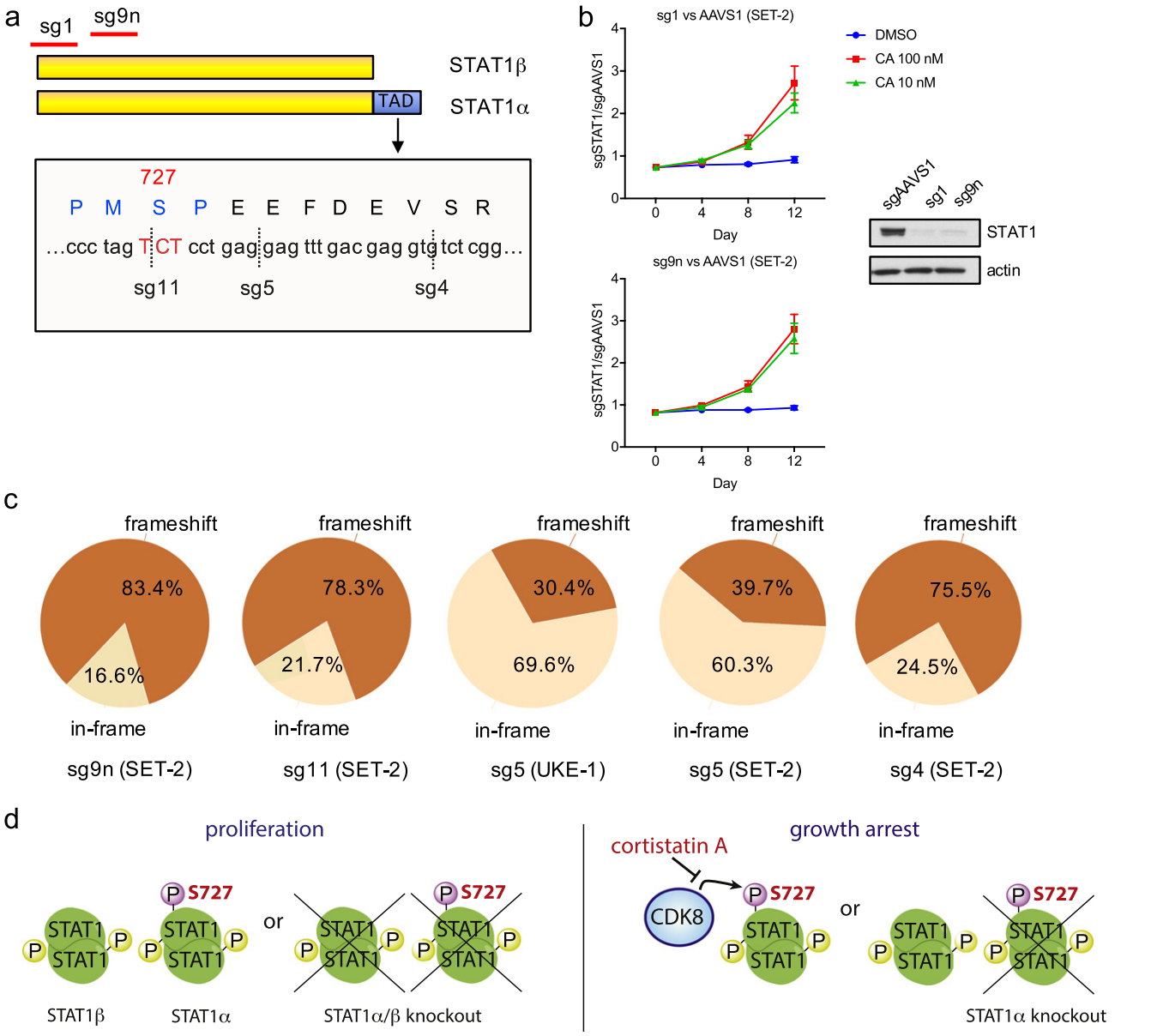

Fig. 3. Depletion of STAT1α or the STAT1 TAD induces growth arrest in JAK2-mutant AML cells. A. Diagram depicts location of various sgRNAs used to target STAT1. Dotted lines represent locations of the Cas9 cut site for each guide. Inset, part of the TAD (transactivation domain) DNA and protein sequence, with the CDK8 recognition motif highlighted in blue and serine 727 in red. B. CRISPR-Cas9-mediated knockout (KO) of STAT1 using sg1 and sg9n shows efficient depletion of STAT1 by immunoblot. STAT1-KO (mCherry) cells show resistance to CA compared to control AAVS1-KO (AmCyan) cells (mean ± s.e.m. ratio of n = 3 biological replicates). Representative growth curves shown for experiments repeated at least three times. C. The pie charts represent the percentage of frameshit versus in-frame mutations generated in pools of cells edited with guide sg5, sg4, sg11, or sg9n. SET-2 or UKE-1 cells were edited two independent times with each sgRNA and sequenced; one experiment is shown. D. Model for the role of STAT1 in proliferation. A proliferative state is maintained when STAT1α/β are present or absent. Growth arrest is induced when the TAD of STAT1α is inhibited by CA or when STAT1α is knocked out. See also Figs. S3 and S4.

knockout of the STAT1α isoform using sg5 and identified a single-cell homozygous *STAT1α* KO clone. This clone exhibited impaired viability compared to WT cells or STAT1 KO cells, implying that loss of STAT1α might result in a gain-of-function by the STAT1β isoform to promote growth arrest (Fig. S4C, D). This result suggests that the TAD may contribute to STAT1's role in promoting JAK2-mutant AML cell proliferation, such that knockout of the TAD impairs viability. Indeed, disproportionate *Stat1β* expression compared to *Stat1α* in zebrafish embryos is thought to play a role in myeloid lineage specification during hematopoiesis, and mammalian STAT1β has been shown not to be dominant negative (Song et al., 2011; Semper et al., 2014). Bancerek et al. reported similarities between knockout of *Stat1α* and knockin of *Stat1 S727A* in mouse embryonic fibroblasts, such as reduction of CDK8 recruitment to interferon target genes (Bancerek et al., 2013). Loss of *STAT1α* might thus be similar phenotypically to inhibition of serine phosphorylation in the TAD by CA.

In support of the importance of STAT1-pS727 in the TAD, induction of double-strand breaks (DSB) by CRISPR-Cas9 at several different loci surrounding the CDK8-recognition motif (PMSP) led to biased enrichment of in-frame repairs that preserve the motif. In non-homologous end joining (NHEJ)-mediated repair, about 66% of events result in a frameshift (Shi et al., 2015). By contrast, only 30–40% of NHEJ events around a cut site near S727 (sg5) resulted in a frameshift, suggesting that there is selection pressure against such a frameshift near the PMSP motif (Fig. 3C) (Shi et al., 2015). This is not observed with sgRNAs targeting early exons in the *STAT1* gene (sg1 and sg9n), loci further downstream of the serine motif (sg4), or loci within 1 bp of the serine codon itself (sg11) where any editing events would disrupt the PMSP

motif (Fig. 3C). Taken together, these data indicate that these post-MPN AML cells are dependent on a functional S727 in the transactivation domain of STAT1, and that disruption of this domain either by phosphorylation inhibition with CA or by selective knockout impairs competitive growth (Fig. 3D).

3.4. CDK8/19 Inhibition Increases Expression of Master Lineage-Specifying Factors and STAT1 Target Genes

Inhibition of CDK8/19 disproportionately increases the expression of cell identity genes in AML cells, including SET-2 (Pelish et al., 2015). Global gene expression analysis by RNA-seq at 4 h following treatment with vehicle or 25 nM CA showed that 87% of genes differentially-expressed ≥1.2-fold are upregulated by CA (Table S1, Fig. S5A). Comparison of the gene expression patterns after CA or ruxolitinib treatment in SET-2 cells showed stark differences and an absence of any correlation between the two (Fig. 4A; $R^2 < 0.0001$), with CA relatively modestly perturbing hundreds of genes while ruxolitinib more robustly affected thousands of genes. Genes upregulated by CA in SET-2 cells were enriched in gene ontology terms related to transcription factor activity and differentiation (Fig. 4B). Many of these genes are key regulators of hematopoiesis and differentiation along the erythroid-megakaryocytic axis, including *GFI1*, *ETS1*, *GATA1*, *GATA2*, *LMO2*, *LMO4*, and *MYB*, among others. Indeed, gene set enrichment analysis (GSEA) revealed that many of the genes upregulated by CA significantly overlapped with megakaryocyte-specific gene sets (Fig. 4C). By contrast, genes differentially expressed after ruxolitinib treatment, derived from RNA-seq data from Meyer et al., 2015, did not show significant enrichment in any of these differentiation gene sets (Fig. 4C). These results demonstrate that distinct transcriptional pathways underlie the cytostatic effects of CA versus the cytotoxicity of ruxolitinib on JAK2-mutant AML cells.

CA disproportionately increased expression of STAT1 target genes normally activated by STAT1, but not genes normally repressed by STAT1 (GSEA, Fig. 4D). If STAT1 were maintaining proliferation by

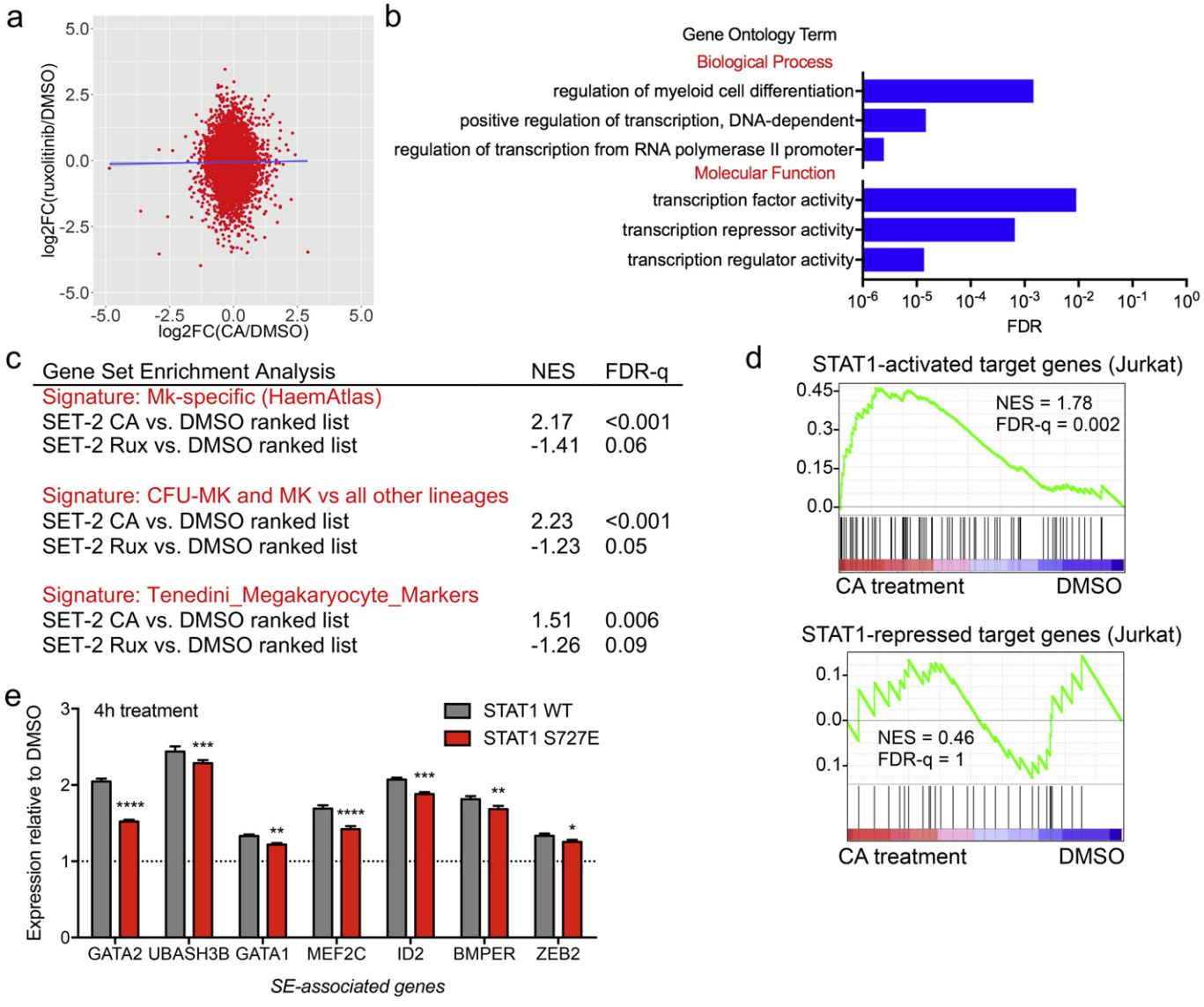

Fig. 4. CA upregulates the expression of differentiation programs in MPN cells, partly through STAT1. A. Scatterplot of differentially expressed genes in SET-2 cells with CA or ruxolitinib treatment (RNA-seq) shows large differences between the transcriptional effects of the two compounds. Ruxolitinib data from Meyer et al., 2015. Best-fit linear regression line in blue, $R^2 = 0.000047$. B. Graph shows enriched molecular function and biological process terms related to transcription factor activity and differentiation from gene ontology analysis (DAVID) of 261 CA-upregulated genes. C. Table shows positive enrichment of three MK differentiation signatures with genes upregulated by CA treatment, but not ruxolitinib treatment (GSEA). D. GSEA plots show that CA upregulates positively-regulated STAT1 target genes, not negatively-regulated STAT1 target genes (published signatures from Sanda et al., 2013). E. STAT1 S727E overexpression (probed for *GATA2*, *UBASH3B*) or knockin (probed for rest) partially rescues upregulation of some SE-associated genes in SET-2 cells by ddPCR (mean ± s.e.m. of Poisson error of two independent experiments, n = 6 biological replicates, two-tailed *t*-tests). See also Fig. S5 and Table S1.

repressing transcription, then knockout should lead to growth inhibition. However, our CRISPR-Cas9 studies showed that JAK2-mutant AML basal growth is not affected by STAT1 knockout (Fig. 3B). Taken together, these data suggest that growth arrest upon inhibition of STAT1 pS727 is mediated primarily by increasing transcription of already-activated STAT1 target genes. A similar phenomenon has been observed in AML cells, where further activation of highly transcribed SE-associated genes can arrest cell growth (Pelish et al., 2015). Overexpression or knockin of the STAT1 S727E mutant was able to partially reverse CA-upregulation of some SE-associated genes compared to STAT1 WT (*GATA2*, *UBASH3B*, *GATA1*, *MEF2C*, *BMPER*, *ID2*, *ZEB2*), but not others (*VEGFA*, *MYB*, *IKZF1*) (Fig. 4E and Fig. S5B). These results show that phosphorylation of STAT1 S727 by CDK8 functions to restrain the expression of a subset of cell identity genes.

3.5. Genome-Wide Mapping of STAT1 pS727 Reveals Occupancy at Super-Enhancers

We sought to further investigate to what extent the transcriptional effects of CDK8/19 inhibition were mediated by STAT1. We performed chromatin immunoprecipitation followed by massively parallel sequencing (ChIP-seq) using a total STAT1 antibody in vehicle or CA-treated cells and a phosphoserine-specific (pS727) STAT1 antibody in untreated cells. Using ChIP-seq to probe the genome-wide localization of post-translationally modified TF species remains challenging due to the difficulty of obtaining high quality datasets with existing antibodies. We validated the selected antibodies by ChIP-qPCR (Fig. S5C) and confirmed that the STAT1 DNA-binding motif was highly enriched in each dataset (Fig. S5D). CA treatment did not induce significant large-scale changes in STAT1 distribution across the genome (Fig. S5E, F). This indicates that blocking S727 phosphorylation does not broadly exclude or recruit STAT1 from chromatin.

We found that STAT1 pS727 was more enriched at gene bodies, which are associated with intragenic enhancers, and less at promoter regions compared to total STAT1 (Fig. S5G). To explore the activity of STAT1 at enhancer regions, we compiled the list of genes associated with the top 500 enhancer-bound peaks of total STAT1 or STAT1 pS727. We then performed GSEAs with the rank-ordered list of differentially expressed genes upon CA treatment. We found that binding of cis-regulatory regions by STAT1 pS727, but not by total STAT1, correlated with CA upregulation (Fig. 5A). Twenty-five genes upregulated ≥1.2-fold (10%) were also associated with the top STAT1 pS727-bound enhancers, including transcription factors *MYB*, *GATA1*, *ID1*, and *LMO2* (Fig. 5B and Fig. S5H). Super-enhancers comprise large stretches of enhancers loaded with transcriptional regulators that drive high expression of cell identity and disease genes. STAT1 pS727 enhancers were also significantly enriched in super-enhancer-associated regions, as determined by H3K27ac (Fig. 5B; *GATA2* locus shown in 5C). These findings suggest that genes with high STAT1 pS727 density at their associated super-enhancers tend to be disproportionately upregulated upon CDK8/19 inhibition. Taken together, these data indicate that CDK8-phosphorylated STAT1 is predominantly loaded at specific cell identity genes to maintain optimal dosage for survival and proliferation in JAK2-mutant AML cells (Fig. 5D).

3.6. CA Reduces Clonogenic Growth of MPN Patient Samples and Allele Burden in an MPN Mouse Model

To more thoroughly gauge the therapeutic potential of CA for MPN patients, we obtained primary patient samples and tested them for sensitivity to CA, ruxolitinib, or both compounds in colony forming unit assays (CFU). We observed dose-dependent reductions in granulocyte-macrophage (CFU-GM) colonies formed by samples treated with CA, in contrast to those treated with ruxolitinib or vehicle (Fig. 6A and Fig. S6A). Furthermore, the colonies that did grow in the presence of CA were smaller (data not shown). Finally, combined ruxolitinib and CA treatment produced fewer colonies than either compound alone. To assess potential toxicity, normal human peripheral blood mononuclear cells (PBMCs) were also treated with either CA, ruxolitinib, vehicle, or CA and ruxolitinib in 1:9 or 1:0.9 ratios, similar to our studies in cell lines (Fig. S6B). At 24 or 72 h, CA, ruxolitinib, or the combination had minimal effects on PBMC viability (multiple comparisons two-way ANOVA vs. DMSO, not significant); in contrast, PBMC viability was strongly impaired with chemotherapeutic agent doxorubicin (Fig. S6C). Concurrently with PBMC viability testing, we also confirmed maximal CDK8/19 and JAK1/2 inhibition (Fig. S6D). At doses of CA and ruxolitinib that fully inhibited CDK8/19 and JAK1/2 in PBMCs, we observed limited effects on PBMC viability. These data suggest that CDK8/CDK19 inhibition, alone or combined with ruxolitinib, has potential to be a promising therapeutic strategy for MPN.

CA is efficacious in a SET-2 xenograft mouse model (Pelish et al., 2015) and we wanted to determine whether CA demonstrated efficacy in other MPN disease models. We tested CA in a *Jak2*V617F knock-in mouse model (Mullally et al., 2010). In this model, bone marrow with a Cre-recombined loxP-flanked *Jak2* V617F allele is transplated in a 1:1 ratio with wild-type bone marrow into lethally-irradiated mice. Recipients develop a lethal MPN characterized by splenomegaly, erythrocytosis, and mild megakaryocyte hyperplasia that is most similar to human PV. We observed that mice treated with 0.16 mg/kg CA daily for 4 weeks had smaller spleens and a significant 25% allele burden reduction compared to vehicle-treated mice (as reflected by the proportion of CD45.2 cells in the bone marrow), unlike mice treated with ruxolitinib (Fig. 6B and Fig. S6E, F). This is comparable to the allele burden reduction seen with MLN8237 at 7 weeks (Wen et al., 2015). We also tested mice with the combination treatment of CA and ruxolitinib. However, the single unoptimized dosage that we tested (0.16 mg/kg CA and 60 mg/kg ruxolitinib daily) was not tolerated, as reflected by body weight loss (data not shown).

4. Discussion

It has been well-documented that MPNs and JAK2-mutant AML cells are sustained by a constitutively activated JAK-STAT pathway through the oncogenic activities of JAK2 and tyrosine-phosphorylated STAT3 and STAT5. Here we found that Mediator kinase inhibition targets a previously unknown dependency of JAK2-mutant neoplasms on STAT1 pS727. This dependency was context-dependent, as certain subsets of JAK2-activated cells did not respond to Mediator kinase inhibition. CRISPR-Cas9 studies targeting the TAD of STAT1 also revealed the importance of this S727-containing domain in maintaining growth in sensitive myeloid cells. These findings are consistent with other reports of serine phosphorylation of STATs as an oncogenic post-translational modification present in many patients with hematological malignancies, among other cancers. For example, expression of phospho-deficient mutant STAT1 S727A ablates the growth of Wilms tumors as well as KRas-induced colon tumors in mice, two contexts in which STAT1 S727 is constitutively phosphorylated (Wang et al., 2016; Wang et al., 2008; Timofeeva et al., 2006). In T-ALL, cells with TYK2 mutations or activated IL-10 signaling (which increase phosphorylated STAT1) have been shown to be dependent on a TYK2-STAT1 pathway (Vahedi et al., 2012; Sanda et al., 2013; Vahedi et al., 2015).

In addition to driving proliferation in hematological malignancies, STAT1 has been implicated in megakaryopoiesis (Huang et al., 2007). In MPN, activated STAT1 signaling is associated with an ET-like phenotype, characterized by increased megakaryopoiesis (Chen et al., 2010). Myelofibrosis, an MPN subtype, is also characterized by overproliferation of abnormal megakaryocytes (Bianchi et al., 2016). In AML, leukemia blast cells experience a block in myeloid differentiation. We found that STAT1 pS727 restrains megakaryocytic differentiation in post-MPN AML cells, and that blocking this phosphorylation by genetic manipulation (mutation to phospho-deficient STAT1 S727A) or pharmacological means (CA treatment) promotes megakaryocytic

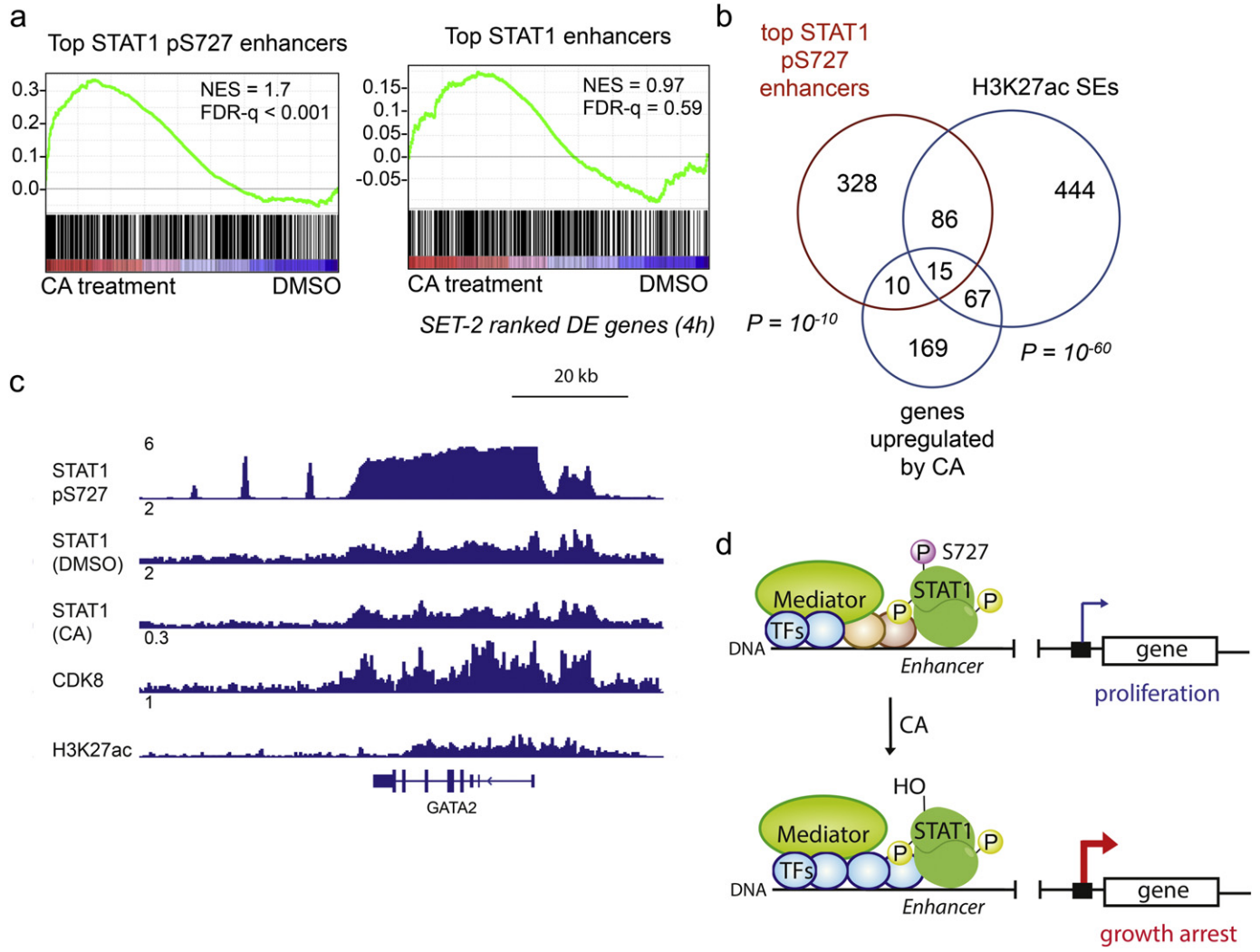

Fig. 5. Genome-wide mapping of STAT1 pS727 reveals occupancy at super-enhancers. A. GSEA plot shows enrichment of CA-upregulated genes in the top non-promoter STAT1 pS727 regions. B. Venn diagram shows the top STAT1 pS727 peaks overlap significantly with genes upregulated by CA (≥1.2-fold), P = 1.05e−10 and H3K27Ac SEs, P = 1.49e−60 (hypergeometric tests). C. ChIP-seq tracks at the *GATA2* locus comparing normalized STAT pS727, total STAT1, CDK8, and H3K27ac signals (in reads per million) in SET-2 cells. D. Model for the mechanism of growth inhibition by CA in JAK-STAT activated neoplasms. See also Fig. S5.

maturation. In contrast, blocking STAT1 tyrosine phosphorylation with ruxolitinib had no effect on megakaryocytic differentiation. Therapeutic benefit in MPN preclinical models has been observed with AURKA inhibitor MLN8237, which also promotes megakaryocytic differentiation (Wen et al., 2015). Thus, Mediator kinase inhibition could target not only proliferation, but also dysregulated differentiation programs driven by STAT1 pS727 in JAK2-mutant neoplasms primed for the megakaryocytic lineage.

Mechanistically, we showed that STAT1 pS727 supports proliferative transcriptional programs and restrains differentiation programs in post-

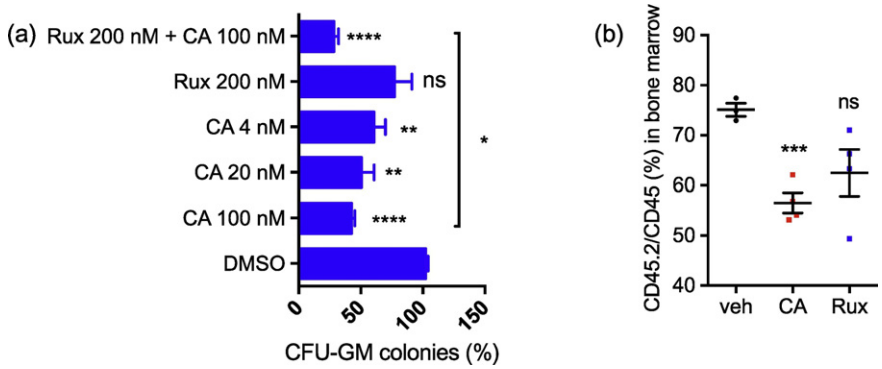

Fig. 6. CA shows efficacy in MPN primary patient samples and MPN mouse model. A. CA alone and in combination with ruxolitinib reduces colony formation in MPN patient samples (each point mean ± s.e.m. of n = 5 patients, two-tailed t-tests). B. Analysis of mutant allele burden in the *Jak2*V617F model showed a significant reduction after 4 weeks of CA 0.16 mg/kg treatment compared to vehicle (n = 3 for vehicle, n = 4 for CA or ruxolitinib, mean ± s.e.m., two-tailed *t*-tests). See also Fig. S6.

MPN AML cells. S727-phosphorylated STAT1 was disproportionally loaded at super-enhancer associated genes, a subset of which were up-regulated upon Mediator kinase inhibition. Many of these genes were associated with transcription factors that promote growth arrest, such as *GATA1* (Elagib et al., 2008; Kuhl et al., 2005), *GATA2* (Shih et al., 2015) and *ID2* (Ghisi et al., 2016), as well as megakaryocyte lineage-specification factors including *PLEK* (Raslova et al., 2007), *CFLAR* (Tenedini, 2004), and *UBASH3B* (Li et al., 2005). STAT1 has been shown to define disease and developmental super-enhancers in another type of leukemia, STAT1-dependent T-ALL (Vahedi et al., 2012; Sanda et al., 2013; Vahedi et al., 2015). We showed that overexpression of phosphomimetic STAT1 S727E can counteract CA-induced upregulation of some SE-associated genes. A model where STAT1 maintains a precise level of a subset of these genes to sustain a proliferative state is consistent with our previous findings showing that AML cells are sensitive to dosage of SE-associated genes (Pelish et al., 2015).

The specific substrates responsible for the anti-proliferative activity of Mediator kinase inhibition in AML had thus far remained unknown. While we found that STAT1 S727 is one downstream substrate in JAK2-mutant cells that mediates the antiproliferative activity of CA, expression of the phosphomimetic mutant STAT1 S727E did not completely reduce sensitivity to CA or abolish all of the transcriptional effects of CDK8/19 inhibition. One possibility is that the phosphomimetic mutant doesn't function as well as true phosphorylated STAT1 (Dephoure et al., 2013). Additionally, other CDK8/19 substrates may contribute to the anti-proliferative effects of CA. Indeed, our studies do not preclude potential contributions of STAT3 and STAT5, which have been reported to be phosphorylated by CDK8/19 on residues S727 and S726, respectively (Bancerek et al., 2013; Rzymski et al., 2017). Furthermore, a phosphoproteomics study with CA revealed Mediator components, transcription factors, and chromatin regulators as putative CDK8/19 substrates (Poss et al., 2016). It will be interesting to determine the role, if any, for these in driving proliferation and survival.

We identified functional differences between serine and tyrosine phosphorylation of STAT1. Ruxolitinib suppressed tyrosine phosphorylation of STAT1 without perturbing serine phosphorylation. Accordingly, the cellular and transcriptional effects of CDK8/19 inhibition were distinct from those of JAK inhibition. The sensitivity of JAK2-activated cells to CDK8/19 inhibition was context-dependent, with our results suggesting a role for lineage background in determining response to CA. Phenotypically, CA induced growth arrest and differentiation in JAK2-mutant AML cells, in contrast to induction of apoptosis with ruxolitinib. In vivo, CA reduced allele burden in an animal model of MPN, unlike ruxolitinib. Moreover, ruxolitinib-persistent cells were just as sensitive to CA as naïve cells, suggesting that Mediator kinase inhibition is able to overcome JAK inhibitor persistence mechanisms. Indeed, we observed that combined CA and ruxolitinib treatment enhances growth suppression in vitro and in patient samples. This supports a model whereby complete inhibition of STAT1 activation results in increased growth arrest, and suggests potential for combination therapy with JAK1/2 and CDK8/19 inhibitors. Future studies will need to be undertaken to assess whether ruxolitinib and CDK8/19 inhibitor co-treatment is tolerated and efficacious in vivo. It remains to be explored whether such a therapeutic approach could be more broadly applicable to other cancers where STAT1 is constitutively activated.

Funding Sources

This work was supported by a Leukemia and Lymphoma Society Translational Research Program Grant (M.D.S. award 6066-14) and the Starr Cancer Consortium (M.D.S. award 607151-5500000738); fellowships from the Swiss National Science Foundation, Swiss Cancer League, and Huggenberger-Bischoff Foundation for Cancer Research (S.C.M.); and a predoctoral fellowship from the National Science Foundation (I.I.N.).

Conflicts of Interest

The authors declare no competing financial interests.

Author Contributions

I.I.N., H.E.P., and M.D.S. designed the research. I.I.N. performed cell-based and biochemical experiments, and analysed data under guidance from M.D.S. Q.J.W. performed growth and flow cytometry assays with 6133/MPL cells under guidance from J.D.C. S.C.M. performed in vivo studies under guidance from R.L.L. I.I.N. and M.E.L. performed computational biology studies. I.I.N, H.E.P. and M.D.S. wrote the manuscript. M.D.S. supervised the research.

Acknowledgements

We thank Diogo H. Da Silva for discussions and cloning STAT1 plasmids and Hanna Tukachinsky and Anupong Tangpeerachaikul for advice on the manuscript. Lentiviral packaging was completed at the University of Massachusetts Medical School RNAi core facility. We thank Harvard FAS Center for Systems Biology for flow sorting and high-throughput sequencing. We thank Hanna Tukachinsky and Stana Nickolich for carrying out the PBMC viability experiment.

Appendix A. Supplementary data

Supplementary data to this article can be found online at https://doi.org/10.1016/j.ebiom.2017.11.013.

References

Allen, B.L., Taatjes, D.J., 2015. The Mediator complex: a central integrator of transcription. Nat. Rev. Mol. Cell Biol. 16 (3), 155–166.
Aronica, M.G., Brizzi, M.F., Dentelli, P., Rosso, A., Yarden, Y., Pegoraro, L., 1996. p91 STAT1 activation in interleukin-3-stimulated primary acute myeloid leukemia cells. Oncogene 13 (5), 1017–1026.
Bancerek, J., Poss, Z.C., Steinparzer, I., Sedlyarov, V., Pfaffenwimmer, T., Mikulic, I., Dölken, L., Strobl, B., Müller, M., Taatjes, D.J., Kovarik, P., 2013. CDK8 kinase phosphorylates transcription factor STAT1 to selectively regulate the interferon response. Immunity 38 (2), 250–262.
Baxter, E.J., 2005. Acquired mutation of the tyrosine kinase JAK2 in human myeloproliferative disorders. Lancet 365, 1054–1061.
Bianchi, E., Norfo, R., Pennucci, V., Zini, R., Manfredini, R., 2016. Genomic landscape of megakaryopoiesis and platelet function defects. Blood 127 (10), 1249–1259.
Cee, V.J., Chen, D.Y.K., Lee, M.R., Nicolaou, K.C., 2009. Cortistatin A is a high-affinity ligand of protein kinases ROCK, CDK8, and CDK11. Angew. Chem. Int. Ed. 48 (47), 8952–8957.
Chen, E., Beer, P.A., Godfrey, A.L., Ortmann, C.A., Li, J., Costa-Pereira, A.P., Ingle, C.E., Dermitzakis, E.T., Campbell, P.J., Green, A.R., 2010. Distinct clinical phenotypes associated with JAK2V617F reflect differential STAT1 signaling. Cancer Cell 18 (5), 524–535.
Chou, T.-C., 2010. Drug combination studies and their synergy quantification using the Chou-Talalay method. Cancer Res. 70 (2), 440–446.
Decker, T., Kovarik, P., 2000. Serine phosphorylation of STATs. Oncogene 19 (21), 2628–2637.
Dehairs, J., Talebi, A., Cherifi, Y., Swinnen, J.V., 2016. CRISP-ID: decoding CRISPR mediated indels by sanger sequencing. Sci. Rep. 6, 28973.
Dephoure, N., Gould, K.L., Gygi, S.P., Kellogg, D.R., 2013. Mapping and analysis of phosphorylation sites: a quick guide for cell biologists. Mol. Biol. Cell 24 (5), 535–542.
Duek, A., Lundberg, P., Shimizu, T., Grisouard, J., Karow, A., Kubovcakova, L., Hao-Shen, H., Dirnhofer, S., Skoda, R.C., 2014. Loss of Stat1 decreases megakaryopoiesis and favors erythropoiesis in a JAK2-V617F driven mouse model of myeloproliferative neoplasms. Blood 123 (25), 3943–3950.
Elagib, K.E., Mihaylov, I.S., Delehanty, L.L., Bullock, G.C., Ouma, K.D., Caronia, J.F., Gonias, S.L., Goldfarb, A.N., 2008. Cross-talk of GATA-1 and P-TEFb in megakaryocyte differentiation. Blood 112 (13), 4884–4894.
Essers, M.A.G., Offner, S., Blanco-Bose, W.E., Waibler, Z., Kalinke, U., Duchosal, M.A., Trumpp, A., 2009. IFNα activates dormant haematopoietic stem cells in vivo. Nature 458 (7240), 904–908.
Ferrajoli, A., Faderl, S., Ravandi, F., Estrov, Z., 2006. The JAK-STAT pathway: a therapeutic target in hematological malignancies. Curr. Cancer Drug Targets 6 (8), 671–679.
Fridman, J.S., Scherle, P.A., Collins, R., Burn, T.C., Li, Y., Li, J., Covington, M.B., Thomas, B., Collier, P., Favata, M.F., Wen, X., Shi, J., McGee, R., Haley, P.J., Shepard, S., Rodgers, J.D., Yeleswaram, S., Hollis, G., Newton, R.C., Metcalf, B., Friedman, S.M., Vaddi, K., 2010. Selective inhibition of JAK1 and JAK2 is efficacious in rodent models of arthritis: preclinical characterization of INCB028050. J. Immunol. 184 (9), 5298–5307.
Friedbichler, K., Kerenyi, M.A., Kovacic, B., Li, G., Hoelbl, A., Yahiaoui, S., Sexl, V., Mullner, E.W., Fajmann, S., Cerny-Reiterer, S., Valent, P., Beug, H., Gouilleux, F., Bunting, K.D.,

Moriggl, R., 2010. Stat5a serine 725 and 779 phosphorylation is a prerequisite for hematopoietic transformation. Blood 116 (9), 1548–1558.
Funakoshi-Tago, M., Tago, K., Abe, M., Sonoda, Y., Kasahara, T., 2010. STAT5 activation is critical for the transformation mediated by myeloproliferative disorder-associated JAK2 V617F mutant. J. Biol. Chem. 285 (8), 5296–5307.
Furqan, M., Mukhi, N., Lee, B., Liu, D., 2013. Dysregulation of JAK-STAT pathway in hematological malignancies and JAK inhibitors for clinical application. Biomarker Res. 1 (1), 5.
Ghisi, M., Kats, L., Masson, F., Li, J., Kratina, T., Vidacs, E., Gilan, O., Doyle, M.A., Newbold, A., Bolden, J.E., Fairfax, K.A., de Graaf, C.A., Firth, M., Zuber, J., Dickins, R.A., Corcoran, L.M., Dawson, M.A., Belz, G.T., Johnstone, R.W., 2016. Id2 and E proteins orchestrate the initiation and maintenance of MLL-rearranged acute myeloid leukemia. Cancer Cell 30 (1), 59–74.
Gouilleux-gruart, V., Debierre-grockiego, F., Gouilleux, F., Capiod, J.-C., Claisse, J.-F., Delobel, J., Prin, L., 2009. Activated Stat related transcription factors in acute leukemia. Leuk. Lymphoma 28 (1–2), 83–88.
Heinz, S., Benner, C., Spann, N., Bertolino, E., Lin, Y.C., Laslo, P., Cheng, J.X., Murre, C., Singh, H., Glass, C.K., 2010. Simple combinations of lineage-determining transcription factors prime cis-regulatory elements required for macrophage and B cell identities. Mol. Cell 38 (4), 576–589.
Hnisz, D., Abraham, B.J., Lee, T.I., Lau, A., Saint-André, V., Sigova, A.A., Hoke, H.A., Young, R.A., 2013. Super-enhancers in the control of cell identity and disease. Cell 155 (4), 934–947.
Huang, Z., Richmond, T.D., Muntean, A.G., 2007. STAT1 promotes megakaryopoiesis downstream of GATA-1 in mice. J. Clin. Invest. 117, 3890–3899.
Huang, D.W., Sherman, B.T., Lempicki, R.A., 2008. Systematic and integrative analysis of large gene lists using DAVID bioinformatics resources. Nat. Protoc. 4 (1), 44–57.
James, C., Ugo, V., Le Couedic, J.-P., Staerk, J., Delhommeau, F., Lacout, C., Garçon, L., Raslova, H., Berger, R., Bennaceur-Griscelli, A., Villeval, J.-L., Constantinescu, S.N., Casadevall, N., Vainchenker, W., 2005. A unique clonal JAK2 mutation leading to constitutive signalling causes polycythaemia vera. Nat. Cell Biol. 434 (7037), 1144–1148.
Jedidi, A., Marty, C., Oligo, C., Jeanson-Leh, L., Ribeil, J.A., Casadevall, N., Galy, A., Vainchenker, W., Villeval, J.L., 2009. Selective reduction of JAK2V617F-dependent cell growth by siRNA/shRNA and its reversal by cytokines. Blood 114 (9), 1842–1851.
Kharchenko, P.V., Tolstorukov, M.Y., Park, P.J., 2008. Design and analysis of ChIP-seq experiments for DNA-binding proteins. Nat. Biotechnol. 26 (12), 1351–1359.
Kleppe, M., Kwak, M., Koppikar, P., Riester, M., Keller, M., Bastian, L., Hricik, T., Bhagwat, N., McKenney, A.S., Papalexi, E., Abdel-Wahab, O., Rampal, R., Marubayashi, S., Chen, J.J., Romanet, V., Fridman, J.S., Bromberg, J., Teruya-Feldstein, J., Murakami, M., Radimerski, T., Michor, F., Fan, R., Levine, R.L., 2015. JAK-STAT pathway activation in malignant and non-malignant cells contributes to MPN pathogenesis and therapeutic response. Cancer Discov. 5 (3) CD–14–0736–331.
Knapp, D., Hammond, C.A., Aghaeepour, N., Miller, P.H., 2017. Distinct signaling programs control human hematopoietic stem cell survival and proliferation. Blood 129, 307–318.
Koppikar, P., Abdel-Wahab, O., Hedvat, C., Marubayashi, S., Patel, J., Goel, A., Kucine, N., Gardner, J.R., Combs, A.P., Vaddi, K., Haley, P.J., Burn, T.C., Rupar, M., Bromberg, J.F., Heaney, M.L., de Stanchina, E., Fridman, J.S., Levine, R.L., 2010. Efficacy of the JAK2 inhibitor INCB16562 in a murine model of MPLW515L-induced thrombocytosis and myelofibrosis. Blood 115 (14), 2919–2927.
Koppikar, P., Bhagwat, N., Kilpivaara, O., Manshouri, T., Adli, M., Hricik, T., Liu, F., Saunders, L.M., Mullally, A., Abdel-Wahab, O., Leung, L., Weinstein, A., Marubayashi, S., Goel, A., Gönen, M., Estrov, Z., Ebert, B.L., Chiosis, G., Nimer, S.D., Bernstein, B.E., Verstovsek, S., Levine, R.L., 2012. Heterodimeric JAK–STAT activation as a mechanism of persistence to JAK2 inhibitor therapy. Nature 489 (7414), 155–159.
Kralovics, R., Passamonti, F., Buser, A.S., Teo, S.-S., Tiedt, R., Passweg, J.R., Tichelli, A., Cazzola, M., Skoda, R.C., 2005. A gain-of-function mutation of JAK2in myeloproliferative disorders. New Engl. J. Med. 352 (17), 1779–1790.
Kuhl, C., Atzberger, A., Iborra, F., Nieswandt, B., Porcher, C., Vyas, P., 2005. GATA1-mediated megakaryocyte differentiation and growth control can be uncoupled and mapped to different domains in GATA1. Mol. Cell. Biol. 25 (19), 8592–8606.
Langmead, B., Trapnell, C., Pop, M., Salzberg, S.L., 2009. Ultrafast and memory-efficient alignment of short DNA sequences to the human genome. Genome Biol. 10 (3), R25.
Levine, R.L., Wadleigh, M., Cools, J., Ebert, B.L., Wernig, G., Huntly, B.J.P., Boggon, T.J., Wlodarska, I., Clark, J.J., Moore, S., Adelsperger, J., Koo, S., Lee, J.C., Gabriel, S., Mercher, T., D'Andrea, A., Fröhling, S., Döhner, K., Marynen, P., Vandenberghe, P., Mesa, R.A., Tefferi, A., Griffin, J.D., Eck, M.J., Sellers, W.R., Meyerson, M., Golub, T.R., Lee, S.J., Gilliland, D.G., 2005. Activating mutation in the tyrosine kinase JAK2 in polycythemia vera, essential thrombocythemia, and myeloid metaplasia with myelofibrosis. Cancer Cell 7 (4), 387–397.
Li, Z., Godinho, F.J., Klusmann, J.-H., Garriga-Canut, M., Yu, C., Orkin, S.H., 2005. Developmental stage-selective effect of somatically mutated leukemogenic transcription factor GATA1. Nat. Genet. 37 (6), 613–619.
Li, Q., Brown, J.B., Huang, H., Bickel, P.J., 2011. Measuring reproducibility of high-throughput experiments. Ann. Appl. Stat. 5 (3), 1752–1779.
Lin, T.S., Mahajan, S., Frank, D.A., 2000. STAT signaling in the pathogenesis and treatment of leukemias. Oncogene 19 (21), 2496–2504.
Lovén, J., Hoke, H.A., Lin, C.Y., Lau, A., Orlando, D.A., Vakoc, C.R., Bradner, J.E., Lee, T.I., Young, R.A., 2013. Selective inhibition of tumor oncogenes by disruption of super-enhancers. Cell 153 (2), 320–334.
Lu, X., Levine, R., Tong, W., Wernig, G., Pikman, Y., Zarnegar, S., Gilliland, D.G., Lodish, H., 2005. Expression of a homodimeric type I cytokine receptor is required for JAK2V617F-mediated transformation. Proc. Natl. Acad. Sci. 102 (52), 18962–18967.
Lucet, I.S., 2006. The structural basis of Janus kinase 2 inhibition by a potent and specific pan-Janus kinase inhibitor. Blood 107 (1), 176–183.
Mascarenhas, J., Heaney, M.L., Najfeld, V., Hexner, E., Abdel-Wahab, O., Rampal, R., Ravandi, F., Petersen, B., Roboz, G., Feldman, E., Podoltsev, N., Douer, D., Levine, R., Tallman, M., Hoffman, R., 2012. Post-myeloproliferative neoplasm acute myeloid leukemia consortium. Proposed criteria for response assessment in patients treated in clinical trials for myeloproliferative neoplasms in blast phase (MPN-BP): formal recommendations from the post-myeloproliferative neoplasm acute myeloid leukemia consortium. Leuk. Res. 36 (12), 1500–1504.
Mesa, R.A., Tibes, R., 2012. MPN blast phase: clinical challenge and assessing response. Leuk. Res. 36 (12), 1496–1497.
Meyer, S.C., Keller, M.D., Chiu, S., Koppikar, P., Guryanova, O.A., Rapaport, F., Xu, K., Manova, K., Pankov, D., O'Reilly, R.J., Kleppe, M., McKenney, A.S., Shih, A.H., Shank, K., Ahn, J., Papalexi, E., Spitzer, B., Socci, N., Viale, A., Mandon, E., Ebel, N., Andraos, R., Rubert, J., Dammassa, E., Romanet, V., Dölemeyer, A., Zender, M., Heinlein, M., Rampal, R., Weinberg, R.S., Hoffman, R., Sellers, W.R., Hofmann, F., Murakami, M., Baffert, F., Gaul, C., Radimerski, T., Levine, R.L., 2015. CHZ868, a type II JAK2 inhibitor, reverses type I JAK inhibitor persistence and demonstrates efficacy in myeloproliferative neoplasms. Cancer Cell 28 (1), 15–28.
Mootha, V.K., Lindgren, C.M., Eriksson, K.-F., Subramanian, A., Sihag, S., Lehár, J., Puigserver, P., Carlsson, E., Ridderstråle, M., Laurila, E., Houstis, N., Daly, M.J., Patterson, N., Mesirov, J.P., Golub, T.R., Tamayo, P., Spiegelman, B., Lander, E.S., Hirschhorn, J.N., Altshuler, D., Groop, L.C., 2003. PGC-1α-responsive genes involved in oxidative phosphorylation are coordinately downregulated in human diabetes. Nat. Genet. 34 (3), 267–273.
Mullally, A., Lane, S.W., Ball, B., Megerdichian, C., Okabe, R., Al-Shahrour, F., Paktinat, M., Haydu, J.E., Housman, E., Lord, A.M., Wernig, G., Kharas, M.G., Mercher, T., Kutok, J.L., Gilliland, D.G., Ebert, B.L., 2010. Physiological Jak2V617F expression causes a lethal myeloproliferative neoplasm with differential effects on hematopoietic stem and progenitor cells. Cancer Cell 17 (6), 584–596.
Novershtern, N., Subramanian, A., Lawton, L.N., Mak, R.H., Haining, W.N., McConkey, M.E., Habib, N., Yosef, N., Chang, C.Y., Shay, T., Frampton, G.M., Drake, A.C.B., Leskov, I., Nilsson, B., Preffer, F., Dombkowski, D., Evans, J.W., Liefeld, T., Smutko, J.S., Chen, J., Friedman, N., Young, R.A., Golub, T.R., Regev, A., Ebert, B.L., 2011. Densely interconnected transcriptional circuits control cell states in human hematopoiesis. Cell 144 (2), 296–309.
Parampalli Yajnanarayana, S., Stübig, T., Cornez, I., Alchalby, H., Schonberg, K., Rudolph, J., Triviai, I., Wolschke, C., Heine, A., Brossart, P., Kröger, N., Wolf, D., 2015. JAK1/2 inhibition impairs T cell function in vitro and in patients with myeloproliferative neoplasms. Br. J. Haematol. 169 (6), 824–833.
Pardanani, A.D., Levine, R.L., Lasho, T., Pikman, Y., Mesa, R.A., Wadleigh, M., Steensma, D.P., Elliott, M.A., Wolanskyj, A.P., Hogan, W.J., McClure, R.F., Litzow, M.R., Gilliland, D.G., Tefferi, A., 2006. MPL515 mutations in myeloproliferative and other myeloid disorders: a study of 1182 patients. Blood 108 (10), 3472–3476.
Patricelli, M.P., Nomanbhoy, T.K., Wu, J., Brown, H., Zhou, D., Zhang, J., Jagannathan, S., Aban, A., Okerberg, E., Herring, C., Nordin, B., Weissig, H., Yang, Q., Lee, J.-D., Gray, N.S., Kozarich, J.W., 2011. In situ kinase profiling reveals functionally relevant properties of native kinases. Chem. Biol. 18 (6), 699–710.
Pelish, H.E., Liau, B.B., Nitulescu, I.I., Tangpeerachaikul, A., Poss, Z.C., Da Silva, D.H., Caruso, B.T., Arefolov, A., Fadeyi, O., Christie, A.L., Du, K., Banka, D., Schneider, E.V., Jestel, A., Zou, G., Si, C., Ebmeier, C.C., Bronson, R.T., Krivtsov, A.V., Myers, A.G., Kohl, N.E., Kung, A.L., Armstrong, S.A., Lemieux, M.E., Taatjes, D.J., Shair, M.D., 2015. Mediator kinase inhibition further activates super-enhancer-associated genes in AML. Nature 526 (7572), 273–276.
Pikman, Y., Lee, B.H., Mercher, T., McDowell, E., Ebert, B.L., Gozo, M., Cuker, A., Wernig, G., Moore, S., Galinsky, I., DeAngelo, D.J., Clark, J.J., Lee, S.J., Golub, T.R., Wadleigh, M., Gilliland, D.G., Levine, R.L., 2006. MPLW515L is a novel somatic activating mutation in myelofibrosis with myeloid metaplasia. PLoS Med. 3 (7), e270.
Pinello, L., Canver, M.C., Hoban, M.D., Orkin, S.H., Kohn, D.B., Bauer, D.E., Yuan, G.-C., 2016. Analyzing CRISPR genome-editing experiments with CRISPResso. Nat. Biotechnol. 34 (7), 695–697.
Poss, Z.C., Ebmeier, C.C., Odell, A.T., Tangpeerachaikul, A., Lee, T., Pelish, H.E., Shair, M.D., Dowell, R.D., Old, W.M., Taatjes, D.J., 2016. Identification of mediator kinase substrates in human cells using cortistatin A and quantitative phosphoproteomics. Cell Rep. 15 (2), 436–450.
Putz, E.M., Gotthardt, D., Hoermann, G., Csiszar, A., Wirth, S., Berger, A., Straka, E., Rigler, D., Wallner, B., Jamieson, A.M., Pickl, W.F., Zebedin-Brandl, E.M., Müller, M., Decker, T., Sexl, V., 2013. CDK8-mediated STAT1-S727 phosphorylation restrains NK cell cytotoxicity and tumor surveillance. Cell Rep. 4 (3), 437–444.
Qin, H.R., Kim, H.-J., Kim, J.-Y., Hurt, E.M., Klarmann, G.J., Kawasaki, B.T., Duhagon Serrat, M.A., Farrar, W.L., 2008. Activation of signal transducer and activator of transcription 3 through a phosphomimetic serine 727 promotes prostate tumorigenesis independent of tyrosine 705 phosphorylation. Cancer Res. 68 (19), 7736–7741.
Quinlan, A.R., Hall, I.M., 2010. BEDTools: a flexible suite of utilities for comparing genomic features. Bioinformatics 26 (6), 841–842.
Quintas-Cardama, A., Vaddi, K., Liu, P., Manshouri, T., Li, J., Scherle, P.A., Caulder, E., Wen, X., Li, Y., Waeltz, P., Rupar, M., Burn, T., Lo, Y., Kelley, J., Covington, M., Shepard, S., Rodgers, J.D., Haley, P., Kantarjian, H., Fridman, J.S., Verstovsek, S., 2010. Preclinical characterization of the selective JAK1/2 inhibitor INCB018424: therapeutic implications for the treatment of myeloproliferative neoplasms. Blood 115 (15), 3109–3117.
Raslova, H., Kauffmann, A., Sekkai, D., Ripoche, H., Larbret, F., Robert, T., Le Roux, D.T., Kroemer, G., Debili, N., Dessen, P., Lazar, V., Vainchenker, W., 2007. Interrelation between polyploidization and megakaryocyte differentiation: a gene profiling approach. Blood 109 (8), 3225–3234.
Roder, S., 2001. STAT3 is constitutively active in some patients with polycythemia rubra vera. Exp. Hematol. 29 (6), 694–702.
Rzymski, T., et al., 2017. SEL120-34A is a novel CDK8 inhibitor active in AML cells with high levels of serine phosphorylation of STAT1 and STAT5 transactivation domains. Oncotarget 8 (20), 33779–33795.

Sanda, T., Tyner, J.W., Gutierrez, A., Ngo, V.N., Glover, J., Chang, B.H., Yost, A., Ma, W., Fleischman, A.G., Zhou, W., Yang, Y., Kleppe, M., Ahn, Y., Tatarek, J., Kelliher, M.A., Neuberg, D.S., Levine, R.L., Moriggl, R., Muller, M., Gray, N.S., Jamieson, C.H.M., Weng, A.P., Staudt, L.M., Druker, B.J., Look, A.T., 2013. TYK2-STAT1-BCL2 pathway dependence in T-cell acute lymphoblastic leukemia. Cancer Discov. 3 (5), 564–577.

Schonberg, K., Rudolph, J., Vonnahme, M., Yajnanarayana, S.P., Cornez, I., Hejazi, M., Manser, A., Uhrberg, M., Verbeek, W., Koschmieder, S., Brummendorf, T.H., Brossart, P., Heine, A., Wolf, D., 2015. JAK inhibition impairs NK cell function in myeloproliferative neoplasms. Cancer Res. 75 (11) canres.3198.2014–2199.

Semper, C., Leitner, N.R., Lassnig, C., Parrini, M., Mahlakõiv, T., Rammerstorfer, M., Lorenz, K., Rigler, D., Müller, S., Kolbe, T., Vogl, C., Rülicke, T., Staeheli, P., Decker, T., Müller, M., Strobl, B., 2014. STAT1β is not dominant negative and is capable of contributing to gamma interferon-dependent innate immunity. Mol. Cell. Biol. 34 (12), 2235–2248.

Shi, Junwei, Wang, E., Milazzo, J.P., Wang, Z., Kinney, J.B., Vakoc, C.R., 2015. Discovery of cancer drug targets by CRISPR-Cas9 screening of protein domains. Nat. Biotechnol. 33 (6), 661–667.

Shi, Jiahai, Yuan, B., Hu, W., Lodish, H., 2016. JAK2 V617F stimulates proliferation of erythropoietin-dependent erythroid progenitors and delays their differentiation by activating Stat1 and other nonerythroid signaling pathways. Exp. Hematol. 44 (11), 1044–1058.e5.

Shih, A.H., Jiang, Y., Meydan, C., Shank, K., Pandey, S., Barreyro, L., Antony-Debre, I., Viale, A., Socci, N., Sun, Y., Robertson, A., Cavatore, M., de Stanchina, E., Hricik, T., Rapaport, F., Woods, B., Wei, C., Hatlen, M., Baljevic, M., Nimer, S.D., Tallman, M., Paietta, E., Cimmino, L., Aifantis, I., Steidl, U., Mason, C., Melnick, A., Levine, R.L., 2015. Mutational cooperativity linked to combinatorial epigenetic gain of function in acute myeloid leukemia. Cancer Cell 27 (4), 502–515.

Song, H., Yan, Y.-L., Titus, T., He, X., Postlethwait, J.H., 2011. The role of stat1b in zebrafish hematopoiesis. Mech. Dev. 128 (7–10), 442–456.

Spivak, J.L., 2004. The chronic myeloproliferative disorders: Clonality and clinical heterogeneity. Semin. Hematol. 41, 1–5.

Subramanian, A., Tamayo, P., Mootha, V.K., Mukherjee, S., Ebert, B.L., Gillette, M.A., Paulovich, A., Pomeroy, S.L., Golub, T.R., Lander, E.S., Mesirov, J.P., 2005. Gene set enrichment analysis: a knowledge-based approach for interpreting genome-wide expression profiles. Proc. Nat. Acad. Sci. USA 102 (43), 15545–15550.

Tenedini, E., 2004. Gene expression profiling of normal and malignant CD34-derived megakaryocytic cells. Blood 104 (10), 3126–3135.

Timofeeva, O.A., Plisov, S., Evseev, A.A., Peng, S., Jose-Kampfner, M., Lovvorn, H.N., Dome, J.S., Perantoni, A.O., 2006. Serine-phosphorylated STAT1 is a prosurvival factor in Wilms' tumor pathogenesis. Oncogene 25 (58), 7555–7564.

Trumpp, A., Essers, M., Wilson, A., 2010. Awakening dormant haematopoietic stem cells. Nat. Rev. Immunol. 10 (3), 201–209.

Vahedi, G., Takahashi, H., Nakayamada, S., Sun, H.-W., Sartorelli, V., Kanno, Y., O'Shea, J.J., 2012. STATs shape the active enhancer landscape of T cell populations. Cell 151 (5), 981–993.

Vahedi, G., Kanno, Y., Furumoto, Y., Jiang, K., Parker, S.C.J., Erdos, M.R., Davis, S.R., Roychoudhuri, R., Restifo, N.P., Gadina, M., Tang, Z., Ruan, Y., Collins, F.S., Sartorelli, V., O'Shea, J.J., 2015. Super-enhancers delineate disease-associated regulatory nodes in T cells. Nature 520 (7548), 558–562.

Vainchenker, W., Constantinescu, S.N., 2013. JAK/STAT signaling in hematological malignancies. Oncogene 32 (21), 2601–2613.

Verstovsek, S., Kantarjian, H., 2007. INCB018424, an oral, selective JAK2 inhibitor, shows significant clinical activity in a phase I/II study in patients with primary myelofibrosis (PMF) and post polycythemia vera/essential thrombocythemia myelofibrosis (post-PV/ET MF). Blood 110, 558.

Walz, C., Ahmed, W., Lazarides, K., Betancur, M., Patel, N., Hennighausen, L., Zaleskas, V.M., Etten, R.A.V., 2012. Essential role for Stat5a/b in myeloproliferative neoplasms induced by BCR-ABL1 and JAK2V617F in mice. Blood 119 (15), 3550–3560.

Wang, S., Raven, J.F., Durbin, J.E., Koromilas, A.E., Jin, D.-Y., 2008. Stat1 Phosphorylation Determines Ras Oncogenicity by Regulating p27Kip1. PLoS One 3 (10), e3476.

Wang, S., Darini, C., Desaubry, L., Koromilas, A.E., 2016. STAT1 promotes KRAS colon tumor growth and susceptibility to pharmacological inhibition of translation initiation factor eIF4A. Mol. Cancer Ther. 15 (12), 3055–3063.

Watkins, N.A., Gusnanto, A., de Bono, B., De, S., Miranda-Saavedra, D., Hardie, D.L., Angenent, W.G.J., Attwood, A.P., Ellis, P.D., Erber, W., Foad, N.S., Garner, S.F., Isacke, C.M., Jolley, J., Koch, K., Macaulay, I.C., Morley, S.L., Rendon, A., Rice, K.M., Taylor, N., Thijssen-Timmer, D.C., Tijssen, M.R., van der Schoot, C.E., Wernisch, L., Winzer, T., Dudbridge, F., Buckley, C.D., Langford, C.F., Teichmann, S., Gottgens, B., Ouwehand, W.H., On behalf of the Bloodomics Consortium, 2009. A HaemAtlas: characterizing gene expression in differentiated human blood cells. Blood 113 (19), e1–e9.

Weber-Nordt, R.M., Egen, C., Wehinger, J., Ludwig, W., 1996. Constitutive activation of STAT proteins in primary lymphoid and myeloid leukemia cells and in Epstein-Barr virus (EBV)-related lymphoma cell lines. Blood 88, 809–816.

Wen, Q.J., Yang, Q., Goldenson, B., Malinge, S.E.B., Lasho, T., Schneider, R.K., Breyfogle, L.J., Schultz, R., Gilles, L., Koppikar, P., Abdel-Wahab, O., Pardanani, A., Stein, B., Gurbuxani, S., Mullally, A., Levine, R.L., Tefferi, A., Crispino, J.D., 2015. Targeting megakaryocytic-induced fibrosis in myeloproliferative neoplasms by AURKA inhibition. Nat. Med. 21, 1473–1480.

Yan, D., Hutchison, R.E., Mohi, G., 2012. Critical requirement for Stat5 in a mouse model of polycythemia vera. Blood 119 (15), 3539–3549.

Zhang, Y., Liu, T., Meyer, C.A., Eeckhoute, J., Johnson, D.S., Bernstein, B.E., Nusbaum, C., Myers, R.M., Brown, M., Li, W., Liu, X.S., 2008. Model-based analysis of ChIP-Seq (MACS). Genome Biol. 9 (9), R137.

Zhao, R., Xing, S., Li, Z., Fu, X., Li, Q., Krantz, S.B., Zhao, Z.J., 2005. Identification of an acquired JAK2 mutation in polycythemia Vera. J. Biol. Chem. 280 (24), 22788–22792.